H-BOX METHODS FOR THE APPROXIMATION OF HYPERBOLIC CONSERVATION LAWS ON IRREGULAR GRIDS

MARSHA J. BERGER*, CHRISTIANE HELZEL*, AND RANDALL J. LEVEQUE†

Abstract. We study a generalization of the high-resolution wave propagation algorithm for the approximation of hyperbolic conservation laws on irregular grids that have a time step restriction based on a reference grid cell length that can be orders of magnitude larger than the smallest grid cell arising in the discretization. This Godunov-type scheme calculates fluxes at cell interfaces by solving Riemann problems defined over boxes of a reference grid cell length h.

We discuss stability, accuracy and entropy consistency of the resulting so-called h-box methods for one-dimensional systems of conservation laws. An extension of the method for the two-dimensional case, that is based on the multidimensional wave propagation algorithm, is also described.

Key words. finite volume methods, hyperbolic conservation laws, non-uniform grids, stability, accuracy, entropy consistency

AMS subject classifications. 35L65, 65M12

1. Introduction.

We consider the numerical approximation of hyperbolic systems of conservation laws using finite volume schemes on irregular grids. We mainly restrict our considerations to the case of one spatial dimension, although an extension to the two dimensional case will also be considered. Under appropriate smoothness assumptions the equations can be formulated in the differential form

$$\frac{\partial}{\partial t} q(x,t) + \frac{\partial}{\partial x} f(q(x,t)) = 0, \tag{1.1}$$

where $q(x,t)$ is a vector of conserved quantities and $f(q(x,t))$ is a vector of flux functions. For the numerical approximation we want to use a finite volume method. On an unstructured grid such a scheme can be written in the general form

$$Q_i^{n+1} = Q_i^n - \frac{\triangle t}{\triangle x_i}\left(F_{i+\frac{1}{2}} - F_{i-\frac{1}{2}}\right), \tag{1.2}$$

where Q_i^n is an approximation of the cell average of the conserved quantity over the grid cell $[x_{i-\frac{1}{2}}, x_{i+\frac{1}{2}}]$ at time $t = t^n$. The vector valued quantities $F_{i-\frac{1}{2}}$ and $F_{i+\frac{1}{2}}$ are the numerical flux functions at the cell interfaces. We denote the time step by $\triangle t$ and the length of the i-th grid cell by $\triangle x_i = x_{i+\frac{1}{2}} - x_{i-\frac{1}{2}}$.

We are in particular interested in the construction of high-resolution schemes for a grid which contains one small grid cell, while all other grid cells have the same length that will be denoted by $h = \triangle x$. This situation is motivated by a two-dimensional application, namely the construction of Cartesian grid methods with embedded irregular geometry. Away from the boundary one may want to use a regular Cartesian grid. Near the boundary one then obtains irregular cut-cells, which may be orders of magnitude smaller than the regular grid cells. Our aim in such a

*Courant Institute of Mathematical Sciences, 251 Mercer Street, New York, NY 10012-1185. `berger@cims.nyu,edu, helzel@cims.nyu.edu` This work was supported by DOE grants DE-FG02-88ER25053 and DE-FC02-01ER25472 and AFOSR grant F49620-00-1-0099.

†Department of Applied Mathematics, University of Washington, Box 352420, Seattle, WA 98195-2420. `rjl@amath.washington.edu` Supported by DOE grants DE-FG03-00ER2592 and DE-FC02-01ER25474 and NSF grant DMS-0106511.

Version of April, 2002

situation is to construct a scheme that is stable based on time steps adequate for the regular grid. Such methods were developed by Berger and LeVeque in [5], [6], [7]. The basic idea of these so-called h-box methods is to approximate the numerical fluxes at the interfaces of a small cell based on initial values specified over regions of length h, i.e. of the length of a regular grid cell. If this is done in an appropriate way then the resulting method remains stable for time steps based on a CFL number that is appropriate for the regular part of the grid. See also [9], [11], [12], [28], [26] and [30] for other embedded boundary Cartesian grid methods that have this same stability property.

Beside this 2D application, h-box schemes can also offer interesting alternatives to existing irregular grid methods. An extension of h-box methods to a completely irregular grid was considered by Berger et. al [8], see also Stern [34]. We will consider such calculations in Section 7. In Section 8, we construct a multidimensional h-box method. Other potential applications for h-box methods are the construction of moving mesh or front-tracking algorithms. Stern [34] used an h-box method to construct a conservative finite volume algorithm for a Cartesian grid with an embedded curvilinear or irregular grid.

Unsurprisingly, the accuracy of an h-box method depends strongly on the definition of the h-box values. In this paper we develop a one-dimensional as well as a two-dimensional high-resolution h-box method. Our goal here is a systematic study of h-box methods in a relatively simple context to provide fundamental understanding for the more complex applications mentioned above. For the advection equation we show that the 1D scheme leads to a second order accurate approximation of smooth solutions on non-uniform grids (without any restrictions on the grid). We also verify that the resulting method leads to high-resolution approximations for the Euler equations on non-uniform meshes. Entropy consistency of the scheme is studied for the approximation of Burgers' equation. The approximation of transonic rarefaction waves turns out to require a special treatment. Throughout this paper we will discuss the construction of h-box methods based on LeVeque's high-resolution wave propagation algorithm [22]. This method is implemented in the CLAWPACK software package [16], which provided the basic tool for our test calculations.

The large time step Godunov method of LeVeque described in [17], [18], [19] is related to the h-box method. This scheme allows larger time steps in the approximation of nonlinear systems of conservation laws by increasing the domain of influence of the numerical scheme. This is done in a wave propagation approach, in which waves are allowed to move through more than one mesh cell. The interaction of waves is approximated by linear superposition. At a reflecting boundary this method becomes more difficult than an h-box method especially in higher dimensions, since the reflection of waves at the boundary has to be considered for waves generated by Riemann problems away from the boundary, see [4]. In [27], Lemma 3.5, Morton showed that high-resolution versions of such a large time step method lead to a second order accurate approximation of the one-dimensional advection equation on a non-uniform grid only if the grid varies smoothly. Our high-resolution h-box method, that will be described in this paper, is superior compared to the large time step Godunov method in the sense that it does not require this smoothness assumption.

For the scalar wave equation $q_{tt} = \nabla^2 q$ the interaction of waves at a small boundary cell can be approximated with high-order accuracy by using the integral formulas developed in Alpert et. al [1]. Numerical methods based on these formulas are currently being developed by Li and Greengard, see [24] for results in one space dimension.

2. The wave propagation algorithm. In this section we describe the basic concept of the high-resolution wave propagation algorithm applied to irregular Cartesian grids; a more general description can be found in LeVeque [22] or [23]. The numerical method for solving (1.1) is a Godunov-type method, i.e. the fluxes at cell interfaces are calculated by solving Riemann problems defined from cell averages of the conserved quantities. This is done by calculating waves that are moving into each grid cell. A first order update calculated by the one-dimensional wave propagation algorithm can be expressed in the form

$$Q_i^{n+1} = Q_i^n - \frac{\triangle t}{\triangle x_i}\left(\mathcal{A}^+\triangle Q_{i-\frac{1}{2}} + \mathcal{A}^-\triangle Q_{i+\frac{1}{2}}\right).$$

Here the change of the conserved quantities is calculated by taking all waves into account that are moving into the grid cell from the left respectively right cell interface. The solution of Riemann problems at cell interfaces provides a decomposition of the jump $Q_{i+1}^n - Q_i^n$ into waves $\mathcal{W}_{i+\frac{1}{2}}^p$ that are moving with speed $s_{i+\frac{1}{2}}^p$ for $p = 1, \ldots, M_w$, i.e.

$$\triangle Q_{i+\frac{1}{2}}^n = Q_{i+1}^n - Q_i^n = \sum_{p=1}^{M_w} \mathcal{W}_{i+\frac{1}{2}}^p.$$

The left- and right-going fluctuations are calculated as

$$\mathcal{A}^+\triangle Q_{i-\frac{1}{2}} = \sum_{p=1}^{M_w} \max(s_{i-\frac{1}{2}}^p, 0)\mathcal{W}_{i-\frac{1}{2}}^p, \quad \mathcal{A}^-\triangle Q_{i+\frac{1}{2}} = \sum_{p=1}^{M_w} \min(s_{i+\frac{1}{2}}^p, 0)\mathcal{W}_{i+\frac{1}{2}}^p.$$

Note that this can be written as a finite volume scheme of the form (1.2) using the relations

$$F_{i+\frac{1}{2}} = f(Q_i) + \mathcal{A}^-\triangle Q_{i+\frac{1}{2}}, \tag{2.1}$$

$$F_{i-\frac{1}{2}} = f(Q_i) - \mathcal{A}^+\triangle Q_{i-\frac{1}{2}}. \tag{2.2}$$

Appropriate waves and speeds for systems of conservation laws can sometimes be calculated by using an exact Riemann solver but more often an approximative Riemann solver, for instance a Roe-Riemann solver [31], is used.

In the wave propagation algorithm second order correction terms are included by extending the first order method into the form

$$Q_i^{n+1} = Q_i^n - \frac{\triangle t}{\triangle x_i}\left(\mathcal{A}^+\triangle Q_{i-\frac{1}{2}} + \mathcal{A}^-\triangle Q_{i+\frac{1}{2}}\right) - \frac{\triangle t}{\triangle x_i}\left(\tilde{F}_{i+\frac{1}{2}}^2 - \tilde{F}_{i-\frac{1}{2}}^2\right). \tag{2.3}$$

On an irregular grid, the second order correction terms have the form

$$\tilde{F}_{i+\frac{1}{2}}^2 = \frac{1}{2}\sum_{p=1}^{M_w} |s_{i+\frac{1}{2}}^p| \left(\frac{\triangle x_i}{\frac{1}{2}(\triangle x_i + \triangle x_{i+1})} - \frac{\triangle t}{\frac{1}{2}(\triangle x_i + \triangle x_{i+1})}|s_{i+\frac{1}{2}}^p|\right)\tilde{\mathcal{W}}_{i+\frac{1}{2}}^p. \tag{2.4}$$

In (2.4) the waves $\tilde{\mathcal{W}}^p$ are limited waves - this limiting is necessary in order to avoid oscillations near discontinuities. For the advection equation $q_t + aq_x = 0$, this high-resolution wave propagation algorithm has a simple geometric interpretation. The update of the conserved quantity Q_i^{n+1} can be obtained by first reconstructing a piecewise linear function

$$\tilde{q}(x,t^n) = Q_i^n + \sigma_i^n(x - x_i) \qquad x \in [x_{i-\frac{1}{2}}, x_{i+\frac{1}{2}}]$$

from the cell averages Q_i^n. The exact solution of the advection equation with these piecewise linear initial values has the form

$$\tilde{q}(x,t^{n+1}) = \tilde{q}(x - a\triangle t, t^n).$$

The cell average of the conserved quantity at the new time t^{n+1} is calculated as

$$Q_i^{n+1} = \frac{1}{\triangle x_i}\int_{x_{i-\frac{1}{2}}}^{x_{i+\frac{1}{2}}} \tilde{q}(x,t^{n+1})dx.$$

For smooth solutions of the advection equation, we can use an unlimited slope of the form

$$\sigma_i^n = \frac{Q_{i+1}^n - Q_i^n}{\frac{1}{2}(\triangle x_i + \triangle x_{i+1})}.$$

This simple reconstruction-evolution-average algorithm for irregular grids can be expressed in the form (2.3), (2.4), see also LeVeque [23].

The resulting numerical scheme is stable as long as time steps are restricted such that waves move through at most one mesh cell, which means the Courant number is no larger than one, i.e.

$$\mathrm{CFL} = \triangle t \max_i \left(\frac{\max(\max_p(s^p_{i-\frac{1}{2}}, 0), |\min_p(s^p_{i+\frac{1}{2}}, 0)|)}{\triangle x_i} \right) \leq 1. \tag{2.5}$$

The h-box method changes this time step restriction by replacing $\triangle x_i$ in the denominator of (2.5) by h, i.e. the width of a reference grid cell. We will use the notation $\mathrm{CFL_h}$ if we want to indicate that the Courant number is based on grid cells of width h.

To illustrate the performance of the high-resolution wave propagation algorithm on an irregular grid we consider a test calculation for the approximation of the advection equation.

EXAMPLE 2.1. *We consider the approximation of the advection equation* $q_t + q_x = 0$ *with initial values* $q(x,0) = \sin(2\pi x)$ *on the interval* $[0,1]$. *Periodic boundary conditions are imposed. We use an irregular grid of the form* $\triangle x_{i+1} = 0.3h$, $\triangle x_{i+2} = 0.4h$, $\triangle x_{i+3} = 0.2h$, $\triangle x_{i+4} = 0.1h$, $\triangle x_{i+5} = 0.5h$, $\triangle x_i + \triangle x_{i+6} = h$, $i = 0, \ldots, mx/10 - 1$, *where* mx *is the number of grid cells used in the discretization and* $h = 2/mx$.

Figure 2.1 (a) shows the numerical and exact solution for Example 2.1 with $h = 0.02$, i.e. we use 100 irregular spaced grid cells. Figure 2.1 (b) documents the experimental order of convergence (EOC) determined by comparing the L_1-error on a sequence of different irregular grids. We obtain a second order accurate approximation on this non-smooth irregular grid, i.e. EOC = 2.02. The time steps were set to satisfy CFL ≤ 0.9.

We want to note that some care is necessary in the construction of second order accurate algorithms for irregular grids. There exist versions of the one-dimensional Lax-Wendroff method which lead to second order accurate approximations of the

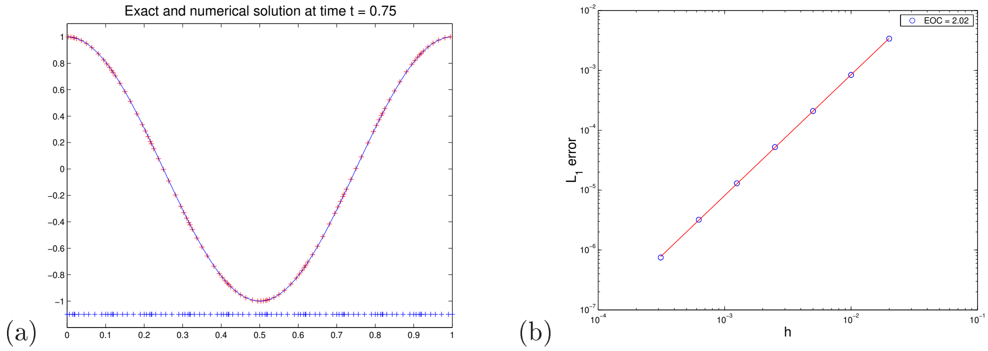

FIG. 2.1. *Approximation of the advection equation on an irregular grid. (a) numerical results on an irregular grid with $h = 0.02$, the irregular grid is shown on the bottom, (b) log-log-plot of h versus L_1-error for high-resolution method, and a linear fit with slope 2.02.*

advection equation only if the grid is sufficiently smooth, i.e. if $\triangle x_i/\triangle x_{i-1} = 1+\mathcal{O}(h)$, ($h = \max_i \triangle x_i$), see for instance Wendroff and White [36], [37] and Pike [29]. See also Morton [27] for convergence results of finite volume methods for the approximation of the advection equation on non-uniform grids.

In the multidimensional case the wave propagation algorithm belongs to the class of truly multidimensional schemes. Here we consider the two-dimensional case, for which a system of conservation laws can be written in the form

$$\frac{\partial}{\partial t}q(x,y,t) + \frac{\partial}{\partial x}f(q(x,y,t)) + \frac{\partial}{\partial y}g(q(x,y,t)) = 0.$$

Instead of using a simple dimension splitting, the wave propagation algorithm accounts for a multidimensional propagation of waves. As in the one-dimensional case, the two-dimensional wave propagation algorithm can be formulated as a finite-volume method that consists of a first order update and a second order correction term. The simplest first order update has the form

$$\begin{aligned} Q_{ij}^{n+1} &= Q_{ij}^n + \triangle_{up} \\ &= Q_{ij}^n - \frac{\Delta t}{\triangle x_{ij}}\left(\mathcal{A}^+\triangle Q_{i-\frac{1}{2},j} + \mathcal{A}^-\triangle Q_{i+\frac{1}{2},j}\right) \\ &\qquad - \frac{\Delta t}{\triangle y_{ij}}\left(\mathcal{B}^+\triangle Q_{i,j-\frac{1}{2}} + \mathcal{B}^-\triangle Q_{i,j+\frac{1}{2}}\right) \end{aligned}$$

The left and right going fluctuations $\mathcal{A}^\pm\triangle Q$ and $\mathcal{B}^\pm\triangle Q$ are calculated in analogy to the 1D case by solving Riemann problems in x as well as in y-direction.

Including the second order correction terms, the method can be expressed in the form

$$Q_{ij}^{n+1} = Q_{ij}^n + \triangle_{up} - \frac{\Delta t}{\triangle x_{ij}}\left(\tilde{F}_{i+\frac{1}{2},j} - \tilde{F}_{i-\frac{1}{2},j}\right) - \frac{\Delta t}{\triangle y_{ij}}\left(\tilde{G}_{i,j+\frac{1}{2}} - \tilde{G}_{i,j-\frac{1}{2}}\right). \qquad (2.6)$$

The multidimensional wave propagation is approximated by defining a transverse propagation of the fluctuations $\mathcal{A}^\pm\triangle Q$ and $\mathcal{B}^\pm\triangle Q$. This is done by splitting each of those fluctuations into two transverse fluctuations, see LeVeque [22] for details of this step. The transverse fluctuations of the left and right-going flux differences are denoted by $\mathcal{B}^+\mathcal{A}^\pm\triangle Q$ and $\mathcal{B}^-\mathcal{A}^\pm\triangle Q$, which corresponds to an up and a down-going part that contributes to the second order correction flux $\tilde{G}$. In order to obtain second order accuracy for irregular grids (without restriction on the mesh), the update of the $\tilde{G}$ flux due to this transverse propagation should have the form:

$$\begin{aligned}
\tilde{G}_{i,j+\frac{1}{2}} &:= \tilde{G}_{i,j+\frac{1}{2}} - \frac{1}{2}\frac{\triangle t}{\triangle x_{ij}}\mathcal{B}^+\mathcal{A}^+\triangle Q_{i-\frac{1}{2},j} \\
\tilde{G}_{i,j-\frac{1}{2}} &:= \tilde{G}_{i,j-\frac{1}{2}} - \frac{1}{2}\frac{\triangle t}{\triangle x_{ij}}\mathcal{B}^-\mathcal{A}^+\triangle Q_{i-\frac{1}{2},j} \\
\tilde{G}_{i-1,j+\frac{1}{2}} &:= \tilde{G}_{i-1,j+\frac{1}{2}} - \frac{1}{2}\frac{\triangle t}{\triangle x_{i-1,j}}\mathcal{B}^+\mathcal{A}^-\triangle Q_{i-\frac{1}{2},j} \\
\tilde{G}_{i-1,j-\frac{1}{2}} &:= \tilde{G}_{i-1,j-\frac{1}{2}} - \frac{1}{2}\frac{\triangle t}{\triangle x_{i-1,j}}\mathcal{B}^-\mathcal{A}^-\triangle Q_{i-\frac{1}{2},j}
\end{aligned} \tag{2.7}$$

Second order corrections of the fluxes calculated in normal direction also have to be incorporated. This can be done by applying another update to the fluxes $\tilde{F}$ and $\tilde{G}$ using formulas analog to (2.4). In Figure 8.2 (c) of Section 8, we show a convergence study for the approximation of the two-dimensional advection equation using this multidimensional wave propagation algorithm. The numerical solution converges with second order accuracy for a sequence of non-smoothly varying irregular grids.

In [23], the implementation of the wave propagation algorithm for conservation laws with capacity function is described in detail. In the one dimensional case a capacity function can be used to account for a non-uniform spaced grid. This leads to the algorithm outlined above. In two space dimensions we have to take into account the grid width as well as the grid length of each grid cell in order to construct a second order wave propagation algorithm for non-uniform grids. This method is not equivalent with the two-dimensional wave propagation algorithm for conservation laws with capacity function. In order to obtain the wave propagation algorithm for irregular grids outlined here, a few simple changes concerning the update (2.6), (2.7) as well as second order correction terms in the form (2.4) have to be made in the original CLAWPACK code.

In this paper we will describe and analyze a new high-resolution wave propagation algorithm which leads to second order accurate approximations of smooth solutions of conservation laws on irregular grids, without any restrictions on the grid. In contrast to the wave propagation algorithm described in this section, this new scheme is stable for time steps that satisfy $\mathrm{CFL}_\mathrm{h} \leq 1$.

3. The one dimensional h-box method. First we want to approximate equation (1.1) on an almost uniform grid that contains one small grid cell in the middle. This situation was also considered by Berger and LeVeque in [5]. This example makes analytical studies a bit easier than the case of a small boundary cell, which is a better model for the embedded Cartesian grid method. However, we will show that the results obtained for this simpler test case can be verified in numerical calculations of more general applications and in particular also in the case where a small cell is located at a reflecting boundary.

We denote the length of a regular grid cell by $h = \triangle x$. The small cell has the length αh, with $0 < \alpha \leq 1$. See Figure 3.1 for further notations that are used in this section. Figure 3.1 (a) shows a small cell (with index k) that is located inside the computational domain. In (b) a small boundary cell (with index 1) is shown; such a situation will be considered in Section 6.

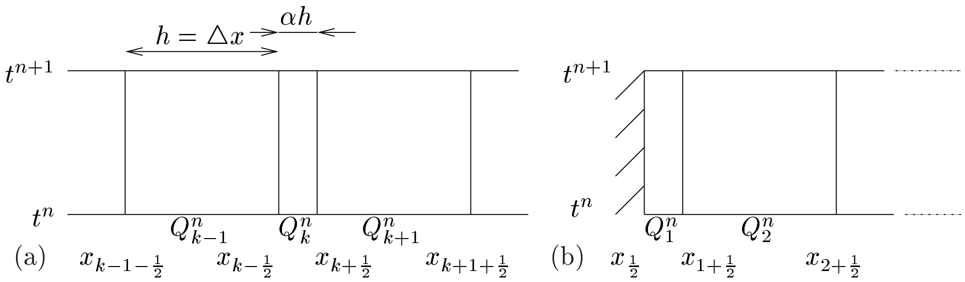

FIG. 3.1. *(a) a small cell inside the computational domain; (b) a small boundary cell*

For the small cell the numerical method has to be modified in order to obtain a stable scheme for time steps $\triangle t$ that satisfy the stability condition in the regular part of the grid. The h-box method introduced by Berger and LeVeque [6] defines new left and right states at the edges of the small cell that represent the conserved quantities at these interfaces over boxes of length h, see Figure 3.2. This guarantees that the domain of dependence of the numerical solution has the size of a regular mesh cell, which is a necessary stability condition. In [6], cell averaging was used in order to calculate these left and right h-box values. It turns out that another interpolation formula leads to much more accurate results. This will be discussed for the advection equation in Sections 3.1 and 3.2 and for the Euler equations in Section 6.

3.1. First order accurate h-box methods. As a first step we compare the performance of two different h-box schemes applied to the advection equation $q_t(x,t) + aq_x(x,t) = 0$. We will assume that $a > 0$, although analogous considerations can of course be made for the case $a < 0$.

In the following we assume that k is the index of the small cell. In order to calculate numerical fluxes at the small cell interface new values of the conserved quantity q, that represent piecewise constant initial values over boxes of length h, will be defined. For the left cell interface of the small cell, these values are denoted by $Q^L_{k-\frac{1}{2}}$ and $Q^R_{k-\frac{1}{2}}$. At the right cell interface of the small cell we have to define values $Q^L_{k+\frac{1}{2}}$ and $Q^R_{k+\frac{1}{2}}$. This is indicated by the shaded boxes at each interface in Figure 3.2.

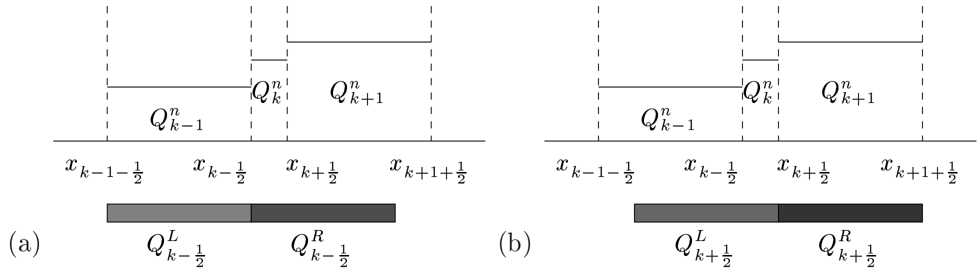

FIG. 3.2. *Schematic description of h-box values assigned to the left small cell interface (see (a)) respectively the right small cell interface (see (b)).*

The most obvious choice is to define the h-box values via cell averaging over the piecewise constant initial values. (To keep the notation simple we sometimes suppress the time index, if it is clear that we mean the values at time t^n.) We obtain:

$$\begin{aligned} Q^L_{k-\frac{1}{2}} &= Q_{k-1}, & Q^R_{k-\frac{1}{2}} &= \alpha Q_k + (1-\alpha) Q_{k+1} \\ Q^L_{k+\frac{1}{2}} &= \alpha Q_k + (1-\alpha) Q_{k-1}, & Q^R_{k+\frac{1}{2}} &= Q_{k+1} \end{aligned} \tag{3.1}$$

Such h-box values were used in Berger and LeVeque [6] as well as by Forrer and Jeltsch [12]. For the advection equation the update of the small cell value can now be calculated using the upwind method. We obtain

$$\begin{aligned} Q^{n+1}_k &= Q^n_k - \frac{\triangle t}{\alpha h}\left(a Q^L_{k+\frac{1}{2}} - a Q^L_{k-\frac{1}{2}}\right) \\ &= Q^n_k - \frac{a \triangle t}{\alpha h}\left(\alpha Q^n_k + (1-\alpha) Q^n_{k-1} - Q^n_{k-1}\right) \\ &= Q^n_k - \frac{a\triangle t}{h}(Q^n_k - Q^n_{k-1}). \end{aligned} \tag{3.2}$$

Note that the small denominator (that may cause a stability problem) has been removed. In Stern [34] stability in the L_1-norm for $\mathrm{CFL_h} \leq 1$ was shown for this h-box method applied to the advection equation, see also Section 4. However, it is clear that this can not be a very accurate formula. The truncation error of the scheme (3.2) has the form

$$\begin{aligned} Lq &= \frac{q^{n+1}_k - q^n_k}{\triangle t} + a\frac{q^n_k - q^n_{k-1}}{h} \\ &= q_t(x_k, t^n) + \frac{a}{2}(\alpha + 1) q_x(x_k, t^n) + \mathcal{O}(\triangle t, h) \\ &= \frac{a}{2}(\alpha - 1) q_x(x_k, t^n) + \mathcal{O}(\triangle t, h) \end{aligned}$$

Only for $\alpha = 1$ is the truncation error in cell k of the order $\mathcal{O}(\triangle t, h)$. Note that grid functions for the exact solution q are expressed with lower case letters, whereas numerical approximations are written in capital letters.

In spite of the apparent inconsistency of the scheme, numerical test calculations suggest that this h-box method converges with first order. For the advection equation we can indeed prove that under appropriate smoothness assumptions the scheme is first order accurate in the small cell. This so-called *supra-convergence property* can be shown using an idea developed for conservation laws by Wendroff and White [36], [37]. See also [15], [25] where these ideas were introduced for boundary value problems for ODEs.

PROPOSITION 1. *We consider the approximation of the advection equation on an almost uniform grid with mesh width h that contains one small mesh cell of length αh, with $\alpha \leq 1$. The 1D h-box method (3.2), that is based on an upwind discretization with h-box values calculated by averaging over piecewise constant cell average values, leads to a first order accurate approximation for sufficiently smooth solutions of the advection equation in spite of the fact that the truncation error indicates inconsistency.*

Proof: The basic step of the proof is to calculate the local truncation error for a grid function w, which must be an accurate enough approximation of the grid function of the exact solution q. We want to show that the truncation error for w is first order, i.e. $Lw = \mathcal{O}(h)$. In order to do this we specify the grid function to have the form

$$w^n_k = q^n_k - \frac{1}{2} h_k q_x(x_k, t^n).$$

The distance between x_k and x_{k-1} respectively x_k and x_{k+1} is $h_{k-\frac{1}{2}} = h_{k+\frac{1}{2}} = \frac{1}{2}h(1+\alpha)$. The length of the small cell is $h_k = \alpha h$ with $0 < \alpha \leq 1$. The truncation error of the grid function w for the scheme (3.2) has the form:

$$\begin{aligned}
Lw &= \frac{w_k^{n+1} - w_k^n}{\triangle t} + a\frac{w_k^n - w_{k-1}^n}{h} \\
&= \frac{q_k^{n+1} - \frac{1}{2}h_k q_x(x_k, t^{n+1}) - q_k^n + \frac{1}{2}h_k q_x(x_k, t^n)}{\triangle t} \\
&+ \ a\frac{q_k^n - \frac{1}{2}h_k q_x(x_k, t^n) - q_{k-1}^n + \frac{1}{2}h q_x(x_{k-1}, t^n)}{h} + \mathcal{O}(\triangle t, h) \\
&= \frac{q_k^n + \triangle t q_t(x_k, t^n) - \frac{1}{2}h_k q_x(x_k, t^n) - q_k^n + \frac{1}{2}h_k q_x(x_k, t^n)}{\triangle t} \\
&+ \ a \ \frac{q_k^n - \frac{1}{2}h_k q_x(x_k, t^n) - q_k^n + h_{k-\frac{1}{2}} q_x(x_k, t^n) + \frac{1}{2}h q_x(x_k, t^n)}{h} + \mathcal{O}(\triangle t, h) \\
&= q_t(x_k, t^n) + q_x(x_k, t^n) a \left(\frac{h_{k-\frac{1}{2}} + \frac{1}{2}h - \frac{1}{2}h_k}{h} \right) + \mathcal{O}(\triangle t, h) \\
&= q_t(x_k, t^n) + a q_x(x_k, t^n) + \mathcal{O}(\triangle t, h) \ = \ \mathcal{O}(\triangle t, h)
\end{aligned}$$

From the truncation error of w and the L_1-norm stability of the method for $\mathrm{CFL_h} \leq 1$ it follows that $|w_k - Q_k| = \mathcal{O}(\triangle t, h)$. Since $w = u + \mathcal{O}(h)$ we obtain the estimate

$$|q_k - Q_k| = \mathcal{O}(h),$$

i.e. the h-box method (3.2) leads to a first order accurate approximation of the advection equation in the small cell k, in spite of the fact that the scheme is inconsistent in the small cell. Using Taylor series expansion one can show that the truncation error Lq in cell $k+1$ is of the order $\mathcal{O}(h)$. In all other regularly spaced grid cells, the method agrees with the upwind scheme for which the truncation error is also $\mathcal{O}(h)$. Therefore, we obtain first order convergence in the whole domain. ∎

In order to obtain a more accurate small cell scheme, we will now consider the construction of h-box values based on linear interpolation using again grid cell values that are overlapped by the h-boxes. Such h-box values have the general form

$$\begin{aligned}
Q_{k-\frac{1}{2}}^L &= Q_{k-1}, & Q_{k-\frac{1}{2}}^R &= \lambda Q_k + (1-\lambda) Q_{k+1} \\
Q_{k+\frac{1}{2}}^L &= \lambda Q_k + (1-\lambda) Q_{k-1}, & Q_{k+\frac{1}{2}}^R &= Q_{k+1}.
\end{aligned}$$

We want to determine λ so that we obtain a consistent h-box scheme, i.e. for which $Lq = \mathcal{O}(h, \triangle t)$. By again using Taylor series expansion we find that only $\lambda = \frac{2\alpha}{1+\alpha}$ leads to an upwind method that satisfies this condition. This suggests that the h-box values should have the form:

$$\begin{aligned}
Q_{k-\frac{1}{2}}^L &= Q_{k-1}, & Q_{k-\frac{1}{2}}^R &= \frac{2\ \alpha\ Q_k + (1-\alpha)\ Q_{k+1}}{1+\alpha} \\
Q_{k+\frac{1}{2}}^L &= \frac{2\ \alpha\ Q_k + (1-\alpha)\ Q_{k-1}}{1+\alpha}, & Q_{k+\frac{1}{2}}^R &= Q_{k+1}.
\end{aligned} \tag{3.3}$$

Note that this interpolation formula was already given in [5], but not further investigated there. In [8], [34] h-box values were defined in a similar way and the resulting scheme was shown to give good results for advection and Burgers' equation.

One time step of the h-box method based on the interpolation formula (3.3) again for $a > 0$ has in the small cell the form

$$\begin{aligned} Q_k^{n+1} &= Q_k^n - \frac{\Delta t}{\alpha h}\left(aQ^L_{k+\frac{1}{2}} - aQ^L_{k-\frac{1}{2}}\right) \\ &= Q_k^n - \frac{a\Delta t}{\alpha h}\left(\frac{2\alpha Q_k + (1-\alpha)Q_{k-1}}{1+\alpha} - Q_{k-1}\right) \\ &= Q_k^n - \frac{a\Delta t}{h}\cdot\frac{Q_k^n - Q_{k-1}^n}{\frac{1+\alpha}{2}}. \end{aligned} \tag{3.4}$$

We can derive the same method as a finite difference scheme, by replacing $q_x(x_k, t^n)$ in the Taylor series expansion of

$$\begin{aligned} q(x_k, t^n + \Delta t) &= q(x_k, t^n) + \Delta t q_t(x_k, t^n) + \mathcal{O}(\Delta t^2) \\ &= q(x_k, t^n) - \Delta t \cdot a\ q_x(x_k, t^n) + \mathcal{O}(\Delta t^2) \end{aligned} \tag{3.5}$$

by an appropriate first order accurate finite difference formula. Taking the different grid cell lengths of cells k and $k-1$ into account, then the spatial derivative $q_x(x_k, t^n)$ can be approximated as

$$q_x(x_k, t^n) = \frac{q(x_k, t^n) - q(x_{k-1}, t^n)}{\overline{h}} + \mathcal{O}(\overline{h}) \qquad \left(\overline{h} = h(1+\alpha)\ /\ 2\right)$$

Including the last formula in (3.5) we obtain

$$q_k^{n+1} = q_k^n - \frac{a\Delta t}{h}\cdot\frac{q_k^n - q_{k-1}^n}{\frac{1+\alpha}{2}} + \mathcal{O}(h^2). \tag{3.6}$$

The first two terms on the right hand side of (3.6) agree with the update of the small cell (3.4) that was obtained by our special construction of h-box values. Therefore, the h-box method (3.4) can be interpreted as a finite difference scheme that approximates the $q_x(x_k)$ terms by one sided finite differences. This h-box method leads to a locally first order accurate method that approximates linear functions exactly. One can also show that an upwind scheme based on the h-box values (3.3) also leads to a consistent first order accurate update in the two neighboring grid cells of the small cell, i.e. in cell $k-1$ (for $a < 0$) and cell $k+1$ (for $a > 0$).

If we use the wave propagation algorithm then the first order update in the small cell can be written in the form

$$Q_k^{n+1} = Q_k^n - \frac{\Delta t}{\alpha h}\left(\mathcal{A}^+\Delta\hat{Q}_{k-\frac{1}{2}} - f(Q^R_{k-\frac{1}{2}}) + \mathcal{A}^-\Delta\hat{Q}_{k+\frac{1}{2}} + f(Q^L_{k+\frac{1}{2}})\right), \tag{3.7}$$

with $\Delta\hat{Q}_{k-\frac{1}{2}} = Q^R_{k-\frac{1}{2}} - Q^L_{k-\frac{1}{2}}$ and $\Delta\hat{Q}_{k+\frac{1}{2}} = Q^R_{k+\frac{1}{2}} - Q^L_{k+\frac{1}{2}}$. In the limit case $\alpha = 1$ we have $Q^R_{k-\frac{1}{2}} = Q^L_{k+\frac{1}{2}}$ and (3.7) reduces to the first order accurate wave propagation algorithm that is valid in the regular parts of the grid. This formula remains valid for nonlinear equations as well as systems of conservation laws, assuming we have a Riemann solver that provides us a decomposition of $Q^R - Q^L$ as described in Section 2. We indicate quantities that are calculated from h-box values by the $\hat{}$ symbol. Example 3.1 shows the different definitions of h-box values in the approximation of the 1D advection equation with sine initial conditions.

EXAMPLE 3.1. *We consider the approximation of the 1D advection equation $q_t + q_x = 0$ on an almost uniform grid that contains one small cell in the middle.*

For our test calculation we start with sine initial values and use periodic boundary conditions. The time steps correspond to $CFL_h = 0.5$. *The small cell is 1.d-5 times the size of a regular cell, i.e.* α = *1.d-5. We consider the numerical solution after one period.*

Figure 3.3 shows numerical results where cell averaging was used in order to define the h-box values. In Figure 3.4 the results of our test problem that were obtained by using the interpolation formula (3.3) are shown. In both cases we also show the error, i.e. the difference of the exact solution minus the numerical solution.

(a) (b)

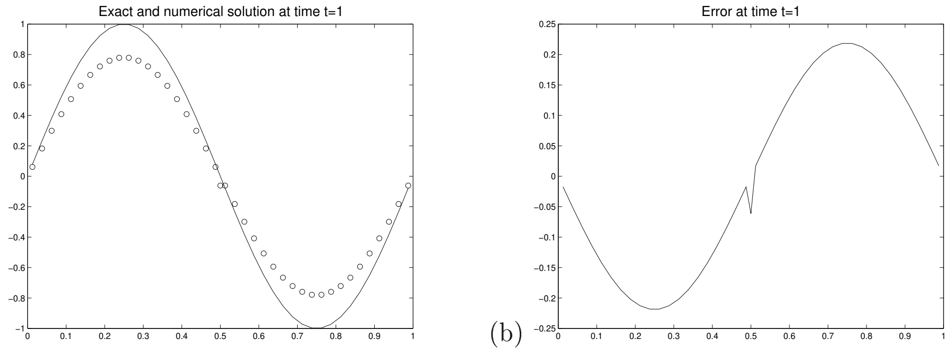

FIG. 3.3. *First order h-box method based on cell averaging with 40 regular grid cells plus one small cell in the middle,* $\alpha = 1.d-5$. *(a) numerical and exact solution, (b) error, i.e. numerical solution minus exact solution.*

(a) (b)

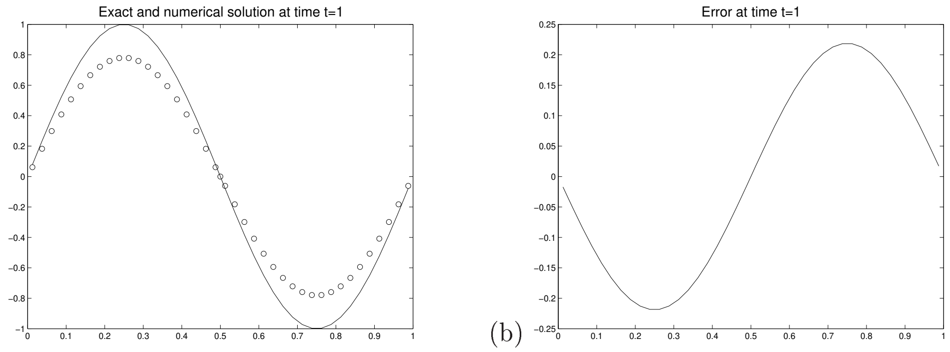

FIG. 3.4. *First order h-box method in which the h-box values are obtained by the interpolation formula (3.3). We use 40 regular grid cells plus one small cell in the middle,* $\alpha = 1.d-5$. *(a) numerical and exact solution, (b) error, i.e. numerical solution minus exact solution.*

3.2. A second order accurate h-box method. In order to obtain a high-resolution scheme we want to include second order correction terms in the form that is used in the wave propagation algorithm for the regular grid cells. This means we want to obtain an update of the small cell that can be written as

$$\begin{aligned} Q_k^{n+1} = Q_k^n &- \frac{\Delta t}{\alpha h}\left(\mathcal{A}^+\triangle\hat{Q}_{k-\frac{1}{2}} - f(Q^R_{k-\frac{1}{2}}) + \mathcal{A}^-\triangle\hat{Q}_{k+\frac{1}{2}} + f(Q^L_{k+\frac{1}{2}})\right)\\ &- \frac{\Delta t}{\alpha h}\left(\hat{F}^2_{k+\frac{1}{2}} - \hat{F}^2_{k-\frac{1}{2}}\right), \end{aligned}$$

here $\hat{F}^2$ denotes the second order correction terms that are implemented in flux differencing form. By analogy to the standard wave propagation algorithm, these second order correction terms should also be calculated by using the waves and speeds obtained from solving Riemann problems at the cell interfaces. For the small cell we again use the waves and speeds from Riemann problems defined by the same h-box values used to obtain the first order update. We will restrict our consideration to h-box values that are calculated using the interpolation formula (3.3).

The formula (2.4) for the second order correction flux on irregular grids suggests using correction terms of the form

$$\hat{F}^2_{i+\frac{1}{2}} = \frac{1}{2}\sum_{p=1}^{M_w}\left(\frac{1}{\frac{1}{2}(1+\alpha)} - \frac{\triangle t}{\frac{1}{2}(1+\alpha)h}|\hat{s}^p_{i+\frac{1}{2}}|\right)\cdot|\hat{s}^p_{i+\frac{1}{2}}|\cdot\hat{\mathcal{W}}^p_{i+\frac{1}{2}} \qquad (i=k-1,\ k) \tag{3.8}$$

in the small cell. The waves $\hat{\mathcal{W}}^p_{i+\frac{1}{2}}$ and the speeds $\hat{s}^p_{i+\frac{1}{2}}$ can be obtained by solving Riemann problems defined by the h-box values at the small cell interfaces. One can show that the truncation error in the small cell that results from such a high-resolution wave propagation scheme is $Lq_k = \mathcal{O}(h^2, \triangle t^2)$, i.e. assuming the scheme is stable we would obtain a second order accurate approximation in the small cell. However, numerical tests showed that such an approach is not stable for time steps satisfying $\mathrm{CFL_h} \leq 1$.

Instead we use second order correction terms of the form:

$$\hat{F}^2_{i+\frac{1}{2}} = \frac{1}{2}\sum_{p=1}^{M_w}\left(1 - \frac{\triangle t}{h}|\hat{s}^p_{i+\frac{1}{2}}|\right)\cdot|\hat{s}^p_{i+\frac{1}{2}}|\hat{\mathcal{W}}^p_{i+\frac{1}{2}} \qquad (i=k-1,\ k) \tag{3.9}$$

Here the waves are again calculated from the Riemann problems defined by the h-box values. The difference to (3.8) is that we don't take the size of the small cell into account in the calculation of the correction fluxes. This reflects the general concept of the h-box method were fluxes are calculated from values defined over regions of length h.

Although the truncation error for the grid cell k now contains first order terms which don't cancel out, the numerical results are very satisfying and indicate second order convergence as well as stability for $\mathrm{CFL_h} \leq 1$. Assuming that the solution is sufficiently smooth we can indeed prove that the resulting method leads to a second order accurate approximation for the advection equation.

PROPOSITION 2. *We consider the approximation of the advection equation on an almost uniform grid with mesh width h that contains one small mesh cell of length αh, with $\alpha \leq 1$. The h-box method consisting of the first order update (3.4) and the second order correction terms (3.9) leads to a second order accurate approximation for sufficiently smooth solutions of the advection equation.*

Proof: We again use the idea of Wendroff and White and consider the truncation error Lw for a grid function of the form $w_i^n = q_i^n + \frac{1}{8}h^2(\alpha_i+1)(\alpha_i-1)q_{xx}(x_i,t^n)$. Here we assume that $h_i = \alpha_i h$. We have $\alpha_i = 1$ for $i \neq k$ and $\alpha_k = \alpha$. In regular grid cells $i \neq k$ the grid function w agrees with the exact solution. We only want to show second order convergence in the small cell as well as in the two neighboring cells $k-1$ and $k+1$, since the method reduces to the high-resolution wave propagation algorithm in the other regular grid cells. In the case considered here, the wave propagation algorithm on the regular part of the grid is equivalent to the Lax-Wendroff scheme.

The truncation error for the grid function w has the form

$$\begin{aligned} Lw &= \frac{w_k^{n+1} - w_k^n}{\Delta t} + 2a\frac{(w_k^n - w_{k-1}^n)}{h(1+\alpha)} + \left(1 - a\frac{\Delta t}{h}\right) a \frac{w_{k+1}^n - 2w_k^n + w_{k-1}^n}{h(1+\alpha)} \\ &= q_t(x_k, t^n) + \frac{\Delta t}{2} q_{tt}(x_k, t^n) + a q_x(x_k, t^n) + \frac{1}{4} h(\alpha - 1) a q_{xx}(x_k, t^n) \\ &\quad - \frac{1}{4} h(1+\alpha) a q_{xx}(x_k, t^n) \\ &\quad + \left(1 - a\frac{\Delta t}{h}\right) a \frac{\frac{1}{4}h^2(1+\alpha)^2 q_{xx}(x_k, t^n) - \frac{1}{4}h^2(\alpha^2 - 1) q_{xx}(x_k, t^n)}{h(1+\alpha)} + \mathcal{O}(\Delta t^2, h^2) \end{aligned}$$

Here we use $h_{k+\frac{1}{2}} = h_{k-\frac{1}{2}} = \frac{1}{2}h(1+\alpha)$ for the distance from the cell center of the small cell k to the cell centers of the neighboring cells. By using the relations $q_t(x_k, t^n) = -a q_x(x_k, t^n)$ and $q_{tt}(x_k, t^n) = a^2 q_{xx}(x_k, t^n)$ all lower order terms in the above equation cancel and we obtain $Lw = \mathcal{O}(\Delta t^2, h^2)$. This shows that $|w_k - Q_k| = \mathcal{O}(\Delta t^2, h^2)$. Since the grid function was chosen to satisfy $w = q + \mathcal{O}(h^2)$, we can conclude that

$$|q_k - Q_k| = \mathcal{O}(\Delta t^2, h^2).$$

Stability of this second order accurate scheme will be shown in the Appendix.

Using the same grid function w, one can also show that $Lw = \mathcal{O}(\Delta t^2, h^2)$ in the neighboring grid cells $k-1$ and $k+1$. Therefore, the numerical solution converges with second order accuracy in the whole domain. ■

Figure 3.5 shows numerical results for Example 3.1 approximated with the high-resolution h-box method. In Table 3.1 we document the experimental order of con-

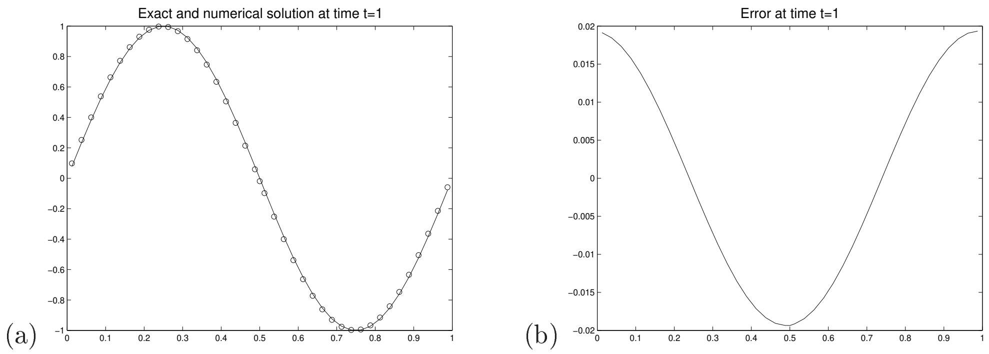

FIG. 3.5. *Second order h-box method defined via linear extrapolation with 40 regular grid cells and one small cell in the middle, $\alpha = 1.d-5$. (a) numerical and exact solution, (b) error, i.e. numerical solution minus exact solution.*

vergence for our test calculation. Figure 3.6 shows a schematic description of the first order update and the high-resolution correction for cell $k+1$. The dotted lines depict the initial values, i.e. $Q^L_{k+\frac{1}{2}}$ and $Q^R_{k+\frac{1}{2}} = Q_{k+1}$. In a first step the piecewise constant values are propagated over a distance $a\Delta t$ as shown in Figure 3.6 (a). In order to increase the accuracy, the piecewise constant initial values are replaced by piecewise linear functions $Q^L_{k+1}(x, t^n)$ and $Q^R_{k+1}(x, t^n)$, see Figure 3.6 (b). The slope

mx / EOC	L_1*-domain error*	*abs. error in small cell*
40+1	0.0118	0.0194
80+1	0.0030	0.0048
EOC	**1.98**	**2.01**
160+1	7.6339d-4	0.0012
EOC	**1.97**	**2.00**
320+1	1.9181d-4	3.0279d-4
EOC	**1.99**	**1.99**

TABLE 3.1
Convergence study for advection problem with small cell in the middle as defined in Example 3.1. Second order correction terms in the small cell are approximated using (3.9).

for the piecewise linear reconstruction $Q^L_{k+\frac{1}{2}}(x,t^n)$ is choosen to be $\sigma = \frac{Q^R_{k+\frac{1}{2}} - Q^L_{k+\frac{1}{2}}}{h}$. Since we already calculated the first order update, the second order correction terms, calculated by propagating piecewise linear initial values $Q^L_{k+\frac{1}{2}}(x,t^n)$ instead of the piecewise constant value $Q^L_{k+\frac{1}{2}}$, only take the shaded region shown in Figure 3.6 (b) into account. Compare with LeVeque [21], where such second order correction terms were described for the approximation of the advection equation on a uniform grid.

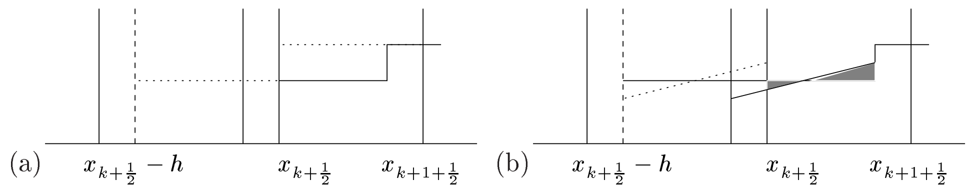

FIG. 3.6. *h-box values at the interface $x_{k+\frac{1}{2}}$, dotted lines depict the initial values, solid lines the solution after one time step. (a) first order update by h-box method, (b) second order correction wave of $Q^L_{i+\frac{1}{2}}$.*

3.3. Limiters for the h-box method. In order to avoid unphysical oscillations near discontinuities some kind of limiters must be used in the second order correction terms (2.4). In the wave propagation algorithm this is done by using *wave limiters*, that modify the magnitude of the waves $\mathcal{W}^p$ ($p = 1, \dots, M_w$) in the fluxes that model the second order correction terms. A limited p-wave $\mathcal{W}^p_{i+\frac{1}{2}}$ is obtained by comparison of this wave with the neighboring p-waves $\mathcal{W}^p_{i-\frac{1}{2}}$ or $\mathcal{W}^p_{i+\frac{3}{2}}$, depending on the direction of flow, see LeVeque [22] or [23] for details.

In our high-resolution h-box method we can use the same limiting process in order to obtain limited versions of the waves that were calculated from h-box values. These limited waves can then be used in the second order correction fluxes (3.9). In order to obtain the limiter for waves at a small cell interface, we compare those waves with waves arising from Riemann problems at a distance h away from the cell interface. This can be done by constructing two additional h-boxes at the small cell interface. The waves resulting from the solution of Riemann problems defined by these new h-box values to the left and right hand side of a small cell interface can then be used in order to estimate the wave limiter for the waves at the small cell interface. This requires the solution of two additional Riemann problems for each small cell interface, see Figure 3.7. We used such a limiting process in order to approximate a shock wave solution on an irregular grid shown in Section 7.

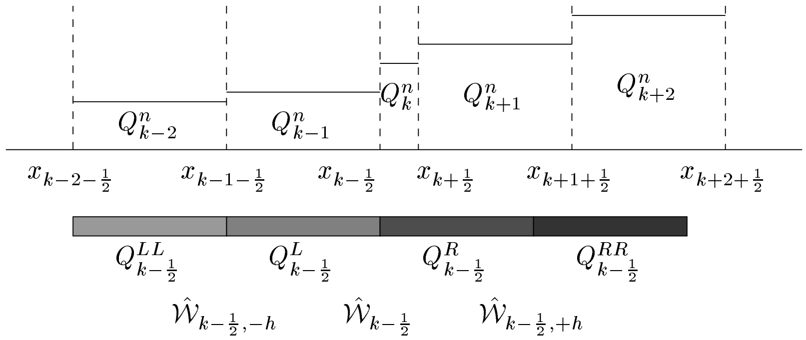

FIG. 3.7. *Schematic description of h-box values assigned to the left small cell interface. Two additional h-box values are needed in order to estimate the wave limiter for the second order correction terms.*

Another somewhat simpler approach is to estimate the waves used in the limiting process from waves that were already calculated. If we have a small cell with index k and length ratio α and an otherwise uniform grid, we can obtain wave limiters for the waves $\hat{\mathcal{W}}^p_{k-\frac{1}{2}}$, $p = 1, \ldots, M_w$ by comparing those waves with estimated neighboring waves $\hat{\mathcal{W}}^p_{k-\frac{1}{2},-h}$ and $\hat{\mathcal{W}}^p_{k-\frac{1}{2},+h}$. In the case of one small cell with index k we can use $\hat{\mathcal{W}}^p_{k-\frac{1}{2},-h} = \mathcal{W}^p_{k-1-\frac{1}{2}}$, since this wave is already located a distance h away from the small cell interface. In order to estimate the wave at the right hand side that is a distance h away from the small cell interface $x_{k-\frac{1}{2}}$, we can use

$$\hat{\mathcal{W}}^p_{k-\frac{1}{2},+h} = \alpha \hat{\mathcal{W}}^p_{k+\frac{1}{2}} + (1-\alpha)\mathcal{W}^p_{k+1+\frac{1}{2}}.$$

Numerical tests (not shown here) confirmed that this simpler limiting process gives also good results and supresses oscillations near discontinuities.

In addition to the wave limiting process we also include a limiter into the approximation of the h-box values. Note that the h-box values (3.3) can also be obtained by reconstructing a piecewise linear function $\overline{Q}(x)$ from the cell average values Q_i for all i and calculating the average value of this piecewise linear function over the same boxes of length h as indicated in Figure 3.2. If the reconstructed function has the form

$$\overline{Q}_{k-1}(x) = Q_{k-1} + \frac{Q_k - Q_{k-1}}{\frac{1}{2}h(1+\alpha)}(x - x_{k-1}) \quad \text{for } x \in [x_{k-\frac{3}{2}}, x_{k-\frac{1}{2}}), \tag{3.10}$$

$$\overline{Q}_{k+1}(x) = Q_{k+1} + \frac{Q_{k+1} - Q_k}{\frac{1}{2}h(1+\alpha)}(x - x_{k+1}) \quad \text{for } x \in [x_{k+\frac{1}{2}}, x_{k+\frac{3}{2}}), \tag{3.11}$$

then averaging over boxes of length h leads to h-box values that have the form (3.3). The slopes of the piecewise linear initial values are

$$\sigma_{k-1} = \frac{Q_k - Q_{k-1}}{\frac{1}{2}h(1+\alpha)} \quad \text{and} \quad \sigma_{k+1} = \frac{Q_{k+1} - Q_k}{\frac{1}{2}h(1+\alpha)}.$$

Near discontinuities such piecewise linear values may not represent a good approximation of the solution. We can use standard *slope limiters* in order to obtain better approximations there. We can for instance use a slope limiter proposed by van Leer [35]. Here the slopes are replaced by limited versions that have the form $\hat{\sigma}_i = \sigma_i \phi_i$ for $i \in \{k-1, k+1\}$. For our application the limiter has the form

$$\phi_i(\theta_i) = \min\left(1, \frac{|\theta_i| + \theta_i}{1 + |\theta_i|}\right)$$

with

$$\theta_{k-1} = \frac{Q_{k-1} - Q_{k-2}}{Q_k - Q_{k-1}} \quad \text{and} \quad \theta_{k+1} = \frac{Q_{k+2} - Q_{k+1}}{Q_{k+1} - Q_k}.$$

It may be replaced by other limiter functions. Note that we don't want to use a steeper slope than σ_{k-1} respectively σ_{k+1} for the construction of h-box values, because only those values lead to a second order approximation in smooth regions. However, near discontinuities we want to limit these slopes. The resulting limited h-box values can be calculated using the formulas

$$\begin{aligned}
Q^L_{k+\frac{1}{2}} &= \alpha Q_k + (1-\alpha)\left(Q_{k-1} + \frac{\alpha}{1+\alpha}(Q_k - Q_{k-1})\phi_{k-1}\right)\\
Q^R_{k-\frac{1}{2}} &= \alpha Q_k + (1-\alpha)\left(Q_{k+1} + \frac{\alpha}{1+\alpha}(Q_k - Q_{k+1})\phi_{k+1}\right).
\end{aligned}$$

4. On the stability of the h-box method. The h-box method retains stability by constructing a finite volume scheme for which the flux difference is of the order of the size of the grid cell. For a small grid cell this requires $F_{k+\frac{1}{2}} - F_{k-\frac{1}{2}} = \mathcal{O}(\alpha h)$. In this case the term αh arising in the denominator of the finite volume scheme should not cause a stability problem. In regions where the solution of the conservation law is smooth, the h-box values are constructed to satisfy an analogous property, namely $Q^{L,R}_{k+\frac{1}{2}} - Q^{L,R}_{k-\frac{1}{2}} = \mathcal{O}(\alpha h)$. Since in our applications the flux function is a Lipschitz continuous function of Q^L and Q^R, the flux difference has the required cancellation property, see [6].

For the advection equation Stern [34] proved that the first order accurate h-box methods are total variation diminishing. Here we will briefly outline this proof which follows the general concept described above. The first order h-box method can (for $a > 0$) be rewritten in the form

$$\begin{aligned}
Q^{n+1}_i &= Q^n_i - \frac{a\triangle t}{\alpha_i h}(Q^L_{i+\frac{1}{2}} - Q^L_{i-\frac{1}{2}})\\
&= Q^n_i - \frac{a\triangle t}{\alpha_i h}\Big(\alpha_i Q^n_i - \underbrace{\alpha_i \int_{x_{i-\frac{1}{2}}-h}^{x_{i-\frac{1}{2}}-h+\alpha_i h} \overline{Q}^n_{i-1}(x)dx}_{\tilde{Q}^n_i}\Big).
\end{aligned}$$

Here we assume that each grid cell has the size $h_i = \alpha_i h$ with $0 < \alpha_i \le 1$. $\overline{Q}^n_{i-1}(x)$ is the piecewise linear reconstructed function (3.10). The stability result also holds on an irregular grid with more than one small cell. See also Section 7 for a slightly different generalization of the piecewise linear function that has to be used in the construction of h-box values for a completely irregular grid.

Using this notation we now consider the difference $|Q_{i+1}^{n+1} - Q_i^{n+1}|$ and sum over all grid cells. This sum can be estimated as:

$$\begin{aligned} TV(Q^{n+1}) &= \sum_i |Q_{i+1}^{n+1} - Q_i^{n+1}| \\ &\leq \left(1 - \frac{a\triangle t}{h}\right) \sum_i |Q_{i+1}^n - Q_i^n| + \frac{a\triangle t}{h} \sum_i |\tilde{Q}_{i+1}^n - \tilde{Q}_i^n| \end{aligned}$$

We obtain the TVD property $TV(Q^{n+1}) \leq TV(Q^n)$ for time steps $\text{CFL}_\text{h} \leq 1$, if

$$\sum_i |\tilde{Q}_{i+1}^n - \tilde{Q}_i^n| \leq TV(Q^n). \tag{4.1}$$

For the h-box method (3.2), based on h-box values that were calculated by averaging over piecewise constant values, inequality (4.1) is always satisfied, since $\tilde{Q}_i^n = Q_i^n$. For the more accurate first order h-box method (3.4), the TVD property can be shown if a TVD slope limiter is used in the construction of the h-box values, as discussed in Section 3.3.

Note that for the approximation of the advection equation, the first order h-box method based on h-box values (3.1), i.e. defined by averaging over piecewise constant values of the conserved quantities is also monotone. This property does not carry over to the first order h-box method with h-box values calculated by the interpolation formula (3.3). Note also that none of these two first order accurate h-box methods applied to Burgers' equation leads to a monotone method.

In the Appendix we show stability for the second order accurate h-box method applied to the advection equation. This proof is based on the stability theory of Gustafsson, Kreiss and Sundstrom [13].

5. Entropy consistency of the h-box method. In this section we study the entropy consistency of the h-box method for Burgers' equation

$$\frac{\partial}{\partial t} q + \frac{\partial}{\partial x}\left(\frac{1}{2}q^2\right) = 0 \tag{5.1}$$

with given initial values $q(x,0)$. We prove that away from sonic points the h-box method with Godunov flux is entropy consistent. The approximation of a transonic rarefaction wave leads to additional difficulties that do not arise in classical Godunov-type schemes.

Entropy consistency can be obtained by showing that an entropy inequality of the form

$$\frac{\partial}{\partial t}\eta(q) + \frac{\partial}{\partial x}\psi(q) \leq 0 \tag{5.2}$$

is satisfied in the weak sense for a convex entropy function $\eta(q)$ and a corresponding consistent entropy flux $\psi(q)$, see for instance [10], [20]. In order to show that a limit solution obtained by a numerical scheme satisfies (5.2), it is sufficient to show that a discrete entropy inequality of the form

$$\eta(Q_i^{n+1}) \leq \eta(Q_i^n) - \frac{\triangle t}{h_i}\left(\Psi_{i+\frac{1}{2}}(Q^n) - \Psi_{i-\frac{1}{2}}(Q^n)\right) \tag{5.3}$$

is satisfied for all i. The numerical entropy flux Ψ has to be consistent with the entropy flux $\eta(q)$. A consistent entropy flux can automatically be obtained if we construct Ψ in an analogous way to the consistent numerical flux F. In this section we analyze first order h-box schemes only. Schonbek [32] showed that an entropy consistent conservative three-point scheme is at most first order accurate.

In the scalar case every convex function can be used as entropy function; we choose $\eta(q) = q^2$. The corresponding entropy flux has the form $\psi(q) = \frac{2}{3}q^3$. Using these functions, a discrete entropy inequality for a first order h-box method for the small cell k can be written in the form

$$\left(Q_k^{n+1}\right)^2 \leq (Q_k^n)^2 - \frac{\triangle t}{h_k}\left[\frac{2}{3}\left(q^*(Q^L_{k+\frac{1}{2}}, Q^R_{k+\frac{1}{2}})\right)^3 - \frac{2}{3}\left(q^*(Q^L_{k-\frac{1}{2}}, Q^R_{k-\frac{1}{2}})\right)^3\right]. \quad (5.4)$$

With $\gamma(k)$ we will denote the entropy production of the numerical scheme in the grid cell k. The entropy production is obtained by subtracting the right hand side of the discrete entropy inequality from the left hand side. Entropy consistency requires that $\gamma(k) \leq 0$ for all k.

Away from a transonic rarefaction wave the exact solution of a Riemann problem for (5.1) at a cell interface has the form

$$q^*(Q_L, Q_R) = \begin{cases} Q_L & : \quad (Q_L + Q_R)/2 > 0 \\ Q_R & : \quad (Q_L + Q_R)/2 < 0. \end{cases} \quad (5.5)$$

5.1. Shock and rarefaction wave solutions away from sonic points. First we consider the cases $Q_{k-1} > Q_k > Q_{k+1} > 0$ which corresponds to a shock wave moving to the right as well as $0 < Q_{k-1} < Q_k < Q_{k+1}$, which leads to a rarefaction wave that is moving to the right. In both cases the solution at a cell interface has the same form, see (5.5). The first order h-box method corresponding to h-box values obtained by the linear interpolation formulas (3.3) has, in the small cell, the form

$$\begin{aligned} Q_k^{n+1} &= Q_k^n - \frac{\Delta t}{\alpha h}\left[\frac{1}{2}\left(Q^L_{k+\frac{1}{2}}\right)^2 - \frac{1}{2}\left(Q^L_{k-\frac{1}{2}}\right)^2\right] \\ &= Q_k^n - \frac{\Delta t}{\alpha h}\left[\frac{1}{2}\left(\frac{2\alpha Q_k^n + (1-\alpha)Q_{k-1}^n}{1+\alpha}\right)^2 - \frac{1}{2}\left(Q_{k-1}^n\right)^2\right] \end{aligned} \quad (5.6)$$

We now consider the discrete entropy production, which takes the form

$$\gamma(k) = \left(Q_k^{n+1}\right)^2 - (Q_k^n)^2 + \frac{\Delta t}{h_k}\left[\frac{2}{3}\left(\frac{2\alpha Q_k^n + (1-\alpha)Q_{k-1}^n}{1+\alpha}\right)^3 - \frac{2}{3}\left(Q_{k-1}^n\right)^3\right],$$

with Q_k^{n+1} calculated from (5.6). After some simplifications we obtain

$$\begin{aligned} \gamma(k) = \Big\{ & 4\triangle t(Q_k^n - Q_{k-1}^n)^2\Big[\alpha Q_k^n\big((\alpha-3)(1+\alpha)h + 3\alpha\triangle t Q_k^n\big) \\ & - \big((1+\alpha)(3+\alpha^2)h - 6\alpha\triangle t Q_k^n\big)Q_{k-1}^n + 3\triangle t(Q_{k-1}^n)^2\Big]\Big\} / \big(3(1+\alpha)^4 h^2\big). \end{aligned} \quad (5.7)$$

In order to show that $\gamma(k) \leq 0$, it is enough to show that the term in squared brackets (that we denote with A) is smaller or equal to zero. First we demonstrate this for data corresponding to a right-going rarefaction wave. Note that the time step restriction for stability requires $\Delta t \le h/Q_k^n \left(\le h/Q_{k-1}^n\right)$. Then we obtain:

$$
\begin{aligned}
A &= Q_k^n h\left(-3\alpha - 2\alpha^2 + \alpha^3\right) + 3\alpha^2 \Delta t (Q_k^n)^2 - Q_{k-1}^n h\left(3 + 3\alpha + \alpha^2 + \alpha^3\right) \\
&\qquad + 6\alpha \Delta t Q_k^n Q_{k-1}^n + 3\Delta t (Q_{k-1}^n)^2 \\
&\le Q_k^n h\left(\alpha^2 - 3\alpha + \alpha^3\right) - Q_{k-1}^n h\left(-3\alpha + \alpha^2 + \alpha^3\right) \\
&= \underbrace{\left(Q_k^n - Q_{k-1}^n\right)}_{\ge 0} \cdot \underbrace{\left(-3h\alpha + \alpha^2 h + \alpha^3 h\right)}_{<0} \\
&\le 0.
\end{aligned}
$$

In the case of a right-going shock wave we use the time step restriction $\Delta t \le h/Q_{k-1}^n \,(\le h/Q_k^n)$. The term in squared brackets can then be estimated as

$$
\begin{aligned}
A &\le Q_k^n h\left(-3\alpha - 2\alpha^2 + \alpha^3\right) + 3\alpha^2 h Q_k^n - Q_{k-1}^n h\left(3 + 3\alpha + \alpha^2 + \alpha^3\right) \\
&\qquad + 6\alpha h Q_k^n + 3h Q_{k-1}^n \\
&= \underbrace{\left(Q_k^n - Q_{k-1}^n\right)}_{\le 0} \cdot \underbrace{\left(3\alpha h + \alpha^2 h + \alpha^3 h\right)}_{>0} \\
&\le 0.
\end{aligned}
$$

Figure 5.1 (a) shows contour plots of $\gamma(k)$ as a function of Q_{k-1}^n and Q_k^n calculated by (5.7). Here we compare the discrete entropy production for the cases (a) $\alpha = 0.05$ and (b) $\alpha = 1$. The time step is calculated such that $\frac{\max(Q_{i-1}, Q_i)\Delta t}{h} = 0.9$. In the

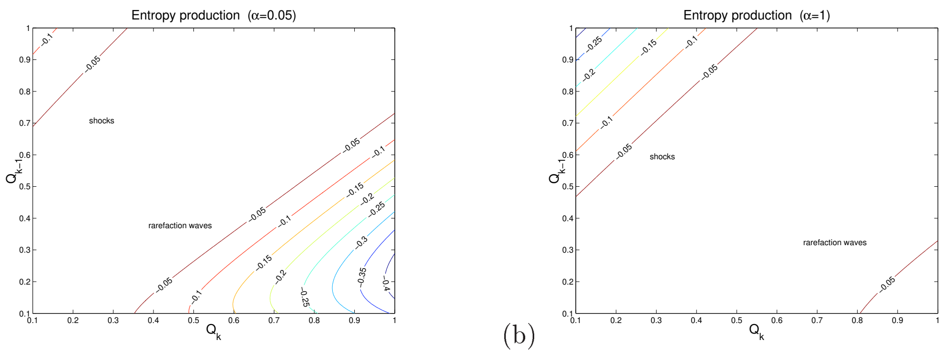

(a) (b)

FIG. 5.1. *Entropy production in the small cell for the first order h-box method (5.6), i.e. in the case of shocks or rarefaction waves moving to the right hand side. (a) $\alpha = 0.05$, (b) $\alpha = 1$.*

small cell the h-box method produces more entropy in the discretization of rarefaction waves compared to the classical Godunov method. Across the shock the scheme (5.6) produces less entropy and as we will discuss in the remark below, this gives us indeed a hint for the construction of the h-box values.

Entropy consistency of shock and rarefaction wave solutions that are moving to the left can be shown in the same way. In order to have a shock as well as a rarefaction wave solution at the interfaces of the small cell, the conserved quantity must have a local minima or maxima in the small cell. Such a solution structure can not persist over several time steps. Instead the solution of the Riemann problems at the cell interfaces of the small cell will either consist of two shock waves or two rarefaction waves.

Remark: In order to show the entropy consistency for the approximation of shock waves we used the time step restriction $\triangle t \leq h/|Q_{k-1}^n|$. This condition was indeed needed in order to show that $\gamma(k) \leq 0$. On a grid cell with $\alpha = 1$ the h-box scheme reduces to Godunov's method. Then we can use $\triangle t = h/0.5(|Q_{i-1}^n|+|Q_i^n|)$, i.e. a time step for which the shock wave moves at most through the whole grid cell. Although the discrete entropy inequality is only a sufficient condition for entropy consistency of the numerical scheme, one can see from test calculations that (by choosing the larger value of $\triangle t$) the h-box method (5.6) can lead to a relatively large error in the small cell during the time step when a shock passes the small cell. In Section 3.3 we noted that near shock waves a slope limiter should be used for the construction of the h-box values. This can also be motivated by looking at the discrete entropy production for the approximation of shock waves. If we use cell averaging over piecewise constant values in order to calculate $Q_{k+\frac{1}{2}}^L$ (say for a shock wave solutions moving to the right), then the discrete entropy production has the form

$$\gamma(k) = \frac{\triangle t}{12h^2}(Q_k^n - Q_{k-1}^n)^2 \Big[\alpha Q_k^n \big(4(2\alpha-3)h + 3\alpha\triangle t Q_k^n\big) \\ -2\big(4\,(3+(\alpha-3)\,\alpha)\,h + 3\,(\alpha-2)\,\alpha\triangle t Q_k^n\big) Q_{k-1}^n + 3(\alpha-2)^2\triangle t (Q_{k-1}^n)^2\Big].$$

Now $\gamma(k) \leq 0$ for time steps $\triangle t \leq h/0.5(Q_k^n + Q_{k-1}^n)$.

5.2. Approximation of transonic rarefaction waves. For piecewise constant initial values that satisfy $Q_L < 0 < Q_R$ the solution of Burgers' equation is a rarefaction wave that spreads over the cell interface. In this situation the solution formula (5.5) is not appropriate. The correct flux at a cell interface for a scalar conservation law with convex flux function in the presence of a rarefaction wave (i.e. for $Q_L \leq Q_R$) can be calculated via the formula

$$F_{i-\frac{1}{2}} = \min_{Q_L \leq q \leq Q_R} f(q). \tag{5.8}$$

For Burgers' equation the h-box method in the small cell k can be written in the form

$$Q_k^{n+1} = Q_k^n - \frac{\triangle t}{\alpha h}\Big(\min_{Q_{k+\frac{1}{2}}^L \leq q \leq Q_{k+\frac{1}{2}}^R} \frac{1}{2}q^2 \;-\; \min_{Q_{k-\frac{1}{2}}^L \leq q \leq Q_{k-\frac{1}{2}}^R} \frac{1}{2}q^2 \Big).$$

These numerical flux functions correspond to the Godunov flux, i.e. to the flux obtained by solving the Riemann problems exactly. It is known that the classical Godunov scheme on a regular grid leads to an entropy consistent approximation, see [14]. By using the Godunov flux in the h-box method we can obtain numerical problems if we approximate transonic rarefaction waves. This will be described in Sections 5.2.1, 5.2.2. In Section 5.2.3 we demonstrate that the numerical problem can be avoided by using the Lax-Friedrichs flux instead of the Godunov flux.

In the case of monotone increasing initial values the relations

$$Q_{k-\frac{1}{2}}^L \leq Q_{k+\frac{1}{2}}^L \leq Q_{k-\frac{1}{2}}^R \leq Q_{k+\frac{1}{2}}^R$$

are valid. We denote with q_* and q_{**} the values which satisfy

$$f(q_*) = \min_{Q_{k-\frac{1}{2}}^L \leq q \leq Q_{k-\frac{1}{2}}^R} \frac{1}{2}q^2 \qquad \text{and} \qquad f(q_{**}) = \min_{Q_{k+\frac{1}{2}}^L \leq q \leq Q_{k+\frac{1}{2}}^R} \frac{1}{2}q^2.$$

Then we obtain for Burgers' equation

$$q_* \leq q_{**}.$$

We now distinguish two possible cases.

5.2.1. Transonic rarefaction wave at the left interface of small cell. For $Q^L_{k-\frac{1}{2}} \leq 0 \leq Q^R_{k-\frac{1}{2}}$ we also have $f(q_*) \leq f(q_{**})$ and therefore the update in the small cell satisfies $Q^{n+1}_k \leq Q^n_k$. For this case we can show that the discrete entropy production is smaller or equal zero:

$$\begin{aligned}\gamma(k) &= \underbrace{(Q^{n+1}_k)^2 - (Q^n_k)^2}_{\leq 0} + \frac{\triangle t}{\alpha h}\underbrace{\left(\frac{2}{3}q_*^3 - \frac{2}{3}q_{**}^3\right)}_{\leq 0} \\ &\leq 0.\end{aligned}$$

In the approximation of transonic rarefaction waves using the h-box method we can obtain a transonic rarefaction wave as the solution of the Riemann problem at the left cell interface as well as at the right cell interface at the same time. Then for both Riemann problems the exact value of the conservative variable at the cell interface is $q = 0$. If this correct solution of the Riemann problem is used in an h-box method we obtain $Q^{n+1}_k = Q^n_k$. In contrast to the Godunov scheme on a regular grid this situation can arise for values $Q^n_k \neq 0$. Nevertheless, we still obtain $\gamma(k) = 0$ in this situation, i.e. the numerical solution converges to the entropy consistent weak solution as the grid becomes sufficiently fine.

5.2.2. Subsonic rarefaction wave at left interface and transonic rarefaction wave at right cell interface. In our last case we consider the situation $Q^L_{k-\frac{1}{2}} \leq Q^R_{k-\frac{1}{2}} \leq 0$ and $Q^L_{k+\frac{1}{2}} \leq 0 \leq Q^R_{k+\frac{1}{2}}$. Here we have $q_* = Q^R_{k-\frac{1}{2}}$ as well as $q_{**} = 0$. Furthermore we know that in order to realize this situation we need $Q^n_k \leq 0$. The update in cell k has the form

$$Q^{n+1}_k = Q^n_k - \frac{\triangle t}{\alpha h}\Big(\frac{1}{2}q_{**}^2 - \frac{1}{2}q_*^2\Big) = Q^n_k + \frac{\triangle t}{\alpha h}\frac{1}{2}(Q^R_{k-\frac{1}{2}})^2.$$

The discrete entropy production takes the form

$$\begin{aligned}\gamma(k) &= (Q^{n+1}_k)^2 - (Q^n_k)^2 + \frac{\triangle t}{\alpha h}\Big(0 - \frac{2}{3}(Q^R_{i-\frac{1}{2}})^3\Big) \\ &= \frac{\triangle t}{\alpha h}Q^n_k(Q^R_{k-\frac{1}{2}})^2 + \frac{1}{4}\frac{\triangle t^2}{\alpha^2 h^2}(Q^R_{k-\frac{1}{2}})^4 - \frac{2}{3}\frac{\triangle t}{\alpha h}(Q^R_{k-\frac{1}{2}})^3 \\ &\leq \frac{\triangle t}{\alpha h}\underbrace{Q^n_k(Q^R_{k-\frac{1}{2}})^2}_{\leq 0} - \frac{1}{4}\frac{\triangle t}{\alpha^2 h}\underbrace{(Q^R_{k-\frac{1}{2}})^3}_{\leq 0} - \frac{2}{3}\frac{\triangle t}{\alpha h}\underbrace{(Q^R_{k-\frac{1}{2}})^3}_{\leq 0}\end{aligned} \tag{5.9}$$

Depending on the strength of the rarefaction wave as well as the size of the parameter α the term on the right hand side of (5.9) can become positive. In this case we have to expect numerical difficulties. As an example, in Figure 5.2 (a) we show the approximation of a transonic rarefaction wave for Burgers' equation on a completely irregular grid. We started the calculation with Riemann initial values $q_L = -0.5$, $q_R = 0.5$. The algorithm used on a completely irregular grid is a generalization of the h-box method for a grid with only one small cell, see Section 7. We use this grid here, because the spurious numerical oscillations that arise in the approximation of transonic rarefaction waves by using the h-box method based on Godunov fluxes become more obvious.

5.2.3. Lax-Friedrichs scheme for the approximation of transonic rarefaction waves. The numerical approximation of transonic rarefaction waves using the h-box method based on the Godunov flux can produce spurious oscillations as shown in Figure 5.2 (a).

It turns out that if the Lax-Friedrichs flux is used in order to calculate the fluxes at the cell interfaces, we obtain an accurate approximation of transonic rarefaction waves. The Lax-Friedrichs flux at the interface $x_{k+\frac{1}{2}}$ has the form

$$F_{k+\frac{1}{2}} = \frac{1}{2}\big(f(Q^L_{k+\frac{1}{2}}) + f(Q^R_{k+\frac{1}{2}})\big) + \frac{h}{2\triangle t}\big(Q^L_{k+\frac{1}{2}} - Q^R_{k+\frac{1}{2}}\big).$$

See Figure 5.2 (b) for a numerical calculation.

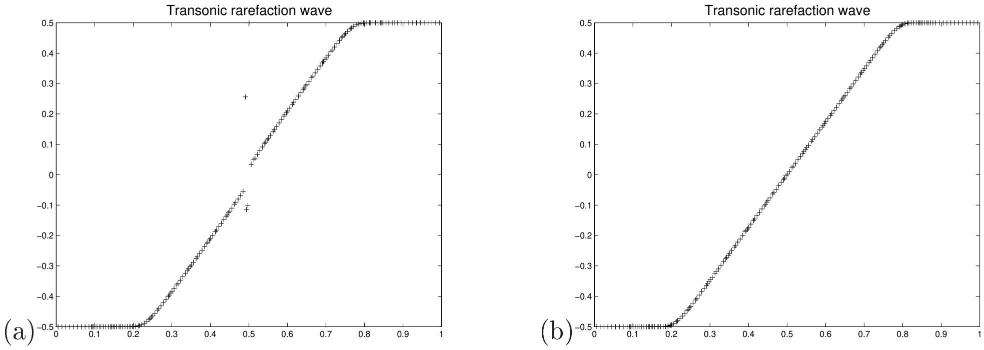

FIG. 5.2. *Approximation of a transonic rarefaction wave solution for Burgers' equation on a completely irregular grid as described in Section 7. (a) h-box method based on Godunov flux, (b) h-box method based on Lax-Friedrichs flux.*

6. Approximation of the Euler equations. In this section we study the performance of the high-resolution h-box method for one-dimensional Euler equations. The equations have the form

$$\begin{aligned} \rho_t + (\rho u)_x &= 0 \\ (\rho u)_t + (\rho u^2 + p)_x &= 0 \\ E_t + (u(E+p))_x &= 0, \end{aligned}$$

where ρ, p, E and u describe the density, pressure, total energy and the velocity respectively. The equation of state has the form

$$E = \frac{p}{\gamma - 1} + \frac{1}{2}\rho u^2.$$

For our numerical calculations we consider the following test case.

EXAMPLE 6.1. *We consider the numerical approximation of the 1D Euler equations on an almost regular grid that contains one small cell in the middle. We choose our initial values sufficiently smooth so that the solution does not develop shocks over the time interval considered. Reflecting boundary conditions are imposed on the left and right boundary. The computational domain is the interval* $[0, 1]$. *Our initial values* *are*

$$
\begin{aligned}
\rho(x,0) &= 1 + 0.4 \sin\left(\frac{\pi}{2} + x\pi\right)\\
u(x,0) &= 0.25 - (x-0.5)^2\\
p(x,0) &= 1
\end{aligned}
$$

The ratio of specific heats is set to $\gamma = 1.4$. The small cell has 0.2 times the length of the regular grid cell, i.e. $\alpha = 0.2$. Time steps are taken so that we have $CFL_h \approx 0.9$ in the regular parts of the grid. In our convergence study we compare the numerical solution on different grids with a numerical solution calculated on a very fine mesh. The highly resolved reference solution is calculated on a regular grid that does not contain a small cell in the center.

We measure the L_1 error of the numerical solution over the whole domain as well as the absolute value of the error in the small cell. The obtained experimental order of convergence is documented for different times in Table 6.1 and results of the numerical calculation are shown in Figure 6.1. As was the case for the advection equation, the

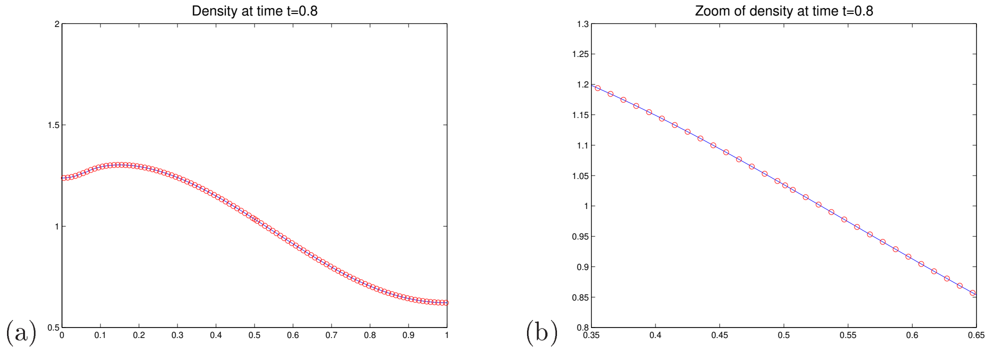

FIG. 6.1. *Numerical results for accuracy test problem approximating Euler equations on a grid with a small cell in the middle using the second order accurate method. The h-box values are defined using the interpolation formula (3.3). (a) plot of density for $mx = 101$, (b) zoom of density plot around the small grid cell that is located at $x = 0.5$.*

numerical results (not shown here) obtained by using the cell averaging formula (3.1) to define h-box values are less accurate. In this case the solution over the domain also converges with second order accuracy in the L_1-norm. In the small cell, an h-box method based on (3.1) that contains the high-resolution correction terms, only converges with first order accuracy. Note that for such an h-box method we can not expect supra-convergence that leads to second order results for the high-resolution h-box method based on (3.3). As we have shown in Section 3.1, the truncation error for the first order update was inconsistent. The supra-convergence result required the existence of a grid function $w = u + \mathcal{O}(h^2)$ with $Lw = \mathcal{O}(h^2)$, in order to show second order convergence. If the first order update however is inconsistent, the grid function w has to contain terms of magnitude $\mathcal{O}(h)$ and therefore one can only hope to obtain first order convergence with such a scheme.

The good performance of the h-box method based on the interpolation formula (3.3) can also be seen if the small cell is located at the boundary. Assuming that the small cell is located at the left boundary (as depicted in Figure 3.1b), we can define

	t=0.2	t = 0.4	t = 0.6	t = 0.8	t = 1
mx/EOC	*L_1 error in density over domain*				
100+1	3.3738d-5	4.4692d-5	7.9737d-5	1.4060d-4	3.5788d-4
200+1	1.0154d-5	1.4159d-5	2.4542d-5	4.1110d-5	1.0771d-4
EOC	**1.73**	**1.63**	**1.70**	**1.77**	**1.73**
400+1	2.8722d-6	4.6013d-6	7.5429d-6	1.1631d-5	3.0600d-5
EOC	**1.82**	**1.62**	**1.70**	**1.82**	**1.82**
mx/EOC	*absolute error in density for small cell*				
100+1	1.0500d-5	0.0011	6.4450d-5	1.8300d-5	2.9760d-5
200+1	2.0500d-6	5.2665d-4	1.4850d-5	4.5000d-6	7.1350d-6
EOC	**2.35**	**1.06**	**2.12**	**2.02**	**2.06**
400+1	4.0000d-7	2.1580d-4	3.7000d-6	1.1000d-6	1.7000d-6
EOC	**2.36**	**1.29**	**2.00**	**2.03**	**2.07**

TABLE 6.1

Convergence study for Euler equations with small cell in the middle. Second order h-box method without limiters.

the h-box values as

$$Q^R_{\frac{1}{2}} = \frac{2\alpha Q_1 + (1-\alpha)Q_2}{1+\alpha}, \qquad Q^L_{\frac{1}{2}} = \mathcal{R} Q^R_{\frac{1}{2}}$$

$$Q^R_{1+\frac{1}{2}} = Q_2, \qquad Q^L_{1+\frac{1}{2}} = \frac{2\alpha Q_1 + (1-\alpha)Q^L_{\frac{1}{2}}}{1+\alpha}.$$

Here $\mathcal{R}$ is the reflection operator that leaves the first and the third component of the vector of conservative quantities constant while negating the second component. Slope limiters may again be incorporated as described in Section 3.3. Results of a numerical convergence study for a test calculation with a small boundary cell, using the same smooth initial values as before, are shown in Table 6.2.

	t=0.2	t = 0.4	t = 0.6	t = 0.8	t = 1
mx/EOC	*L_1 error in density over domain*				
100+1	3.2002d-5	3.9125d-5	7.3907d-5	1.3429d-4	3.4976d-4
200+1	9.6864d-6	1.4020d-5	2.3610d-5	3.9459d-5	1.0653d-4
EOC	**1.72**	**1.48**	**1.65**	**1.77**	**1.72**
400+1	2.7483d-6	4.5213d-6	7.2293d-6	1.1036d-5	3.0546d-5
EOC	**1.82**	**1.63**	**1.71**	**1.84**	**1.80**
mx/EOC	*absolute error in density for small boundary cell*				
100+1	1.6400d-5	1.1325d-5	2.1650d-5	4.0305d-4	4.9545d-4
200+1	4.3500d-6	2.6000d-6	6.0500d-6	1.1965d-4	1.1465d-4
EOC	**1.91**	**2.12**	**1.84**	**1.75**	**2.11**
400+1	1.1000d-6	8.0000d-7	1.5000d-6	3.0800d-5	2.6600d-5
EOC	**1.98**	**1.70**	**2.01**	**1.96**	**2.11**

TABLE 6.2

Convergence study for Euler equations with small boundary cell. Second order h-box method without limiters.

7. Irregular grid calculation. In order to demonstrate the robustness of the high-resolution h-box method we now apply the scheme to a completely arbitrary grid. By again assigning values to boxes of length h, we obtain a scheme that remains stable for time steps appropriate for a uniform grid with grid cells of length h. In this more general situation more than two grid cells may be overlapped by an h-box. We assume that grid cells have the length $h_i = \alpha_i h$ with $\alpha_i \leq 1$ for all indices i. We will show that a generalization of the h-box method based on averaging over piecewise linear values of the conserved quantities gives accurate results also in this more difficult situation. We will need to use piecewise linear reconstructed values

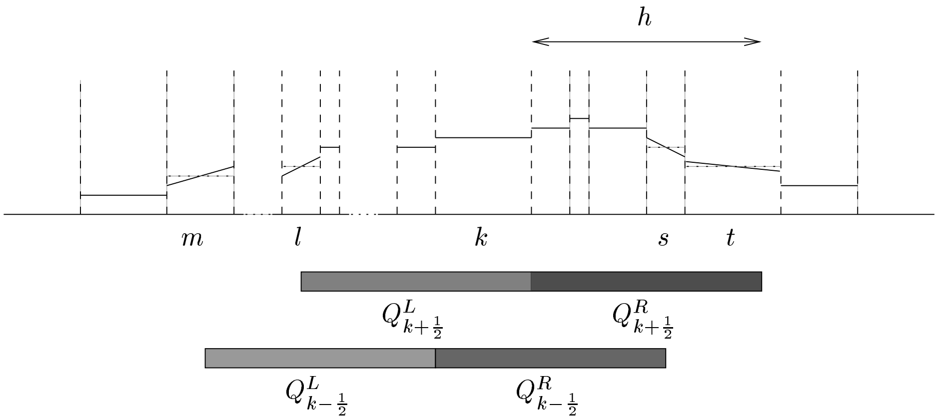

FIG. 7.1. *Schematic description of the h-box method on a completely irregular grid.*

$$\overline{Q}_i(x) = Q_i + \frac{Q_{i+1} - Q_i}{\frac{1}{2}h(\alpha_i + \alpha_{i+1})}(x - x_i) \quad \text{for } x \in [x_{i-\frac{1}{2}}, x_{i+\frac{1}{2}}), \quad i \in \{m, l\} \tag{7.1}$$

$$\overline{Q}_j(x) = Q_j + \frac{Q_j - Q_{j-1}}{\frac{1}{2}h(\alpha_j + \alpha_{j-1})}(x - x_j) \quad \text{for } x \in [x_{j-\frac{1}{2}}, x_{j+\frac{1}{2}}), \quad j \in \{s, t\}. \tag{7.2}$$

The indices m, l and s, t indicate the grid cells that are only partly covered by the left- respectively right-going h-boxes that are constructed at the cell interfaces of grid cell k. Slopes are needed only in these four cells because averaging over an entire cell gives a value that is independent of the slope.

Averaging over these piecewise linear values leads to the h-box values

$$Q^L_{k-\frac{1}{2}} = \sum_{i=m+1}^{k-1} \alpha_i Q_i + \Big(1 - \sum_{i=m+1}^{k-1} \alpha_i\Big) \cdot \Big[Q_m + \frac{Q_{m+1} - Q_m}{\alpha_m + \alpha_{m+1}}\Big(\sum_{i=m}^{k-1} \alpha_i - 1\Big)\Big]$$

$$Q^R_{k-\frac{1}{2}} = \sum_{i=k}^{s-1} \alpha_i Q_i + \Big(1 - \sum_{i=k}^{s-1} \alpha_i\Big) \cdot \Big[Q_s + \frac{Q_s - Q_{s-1}}{\alpha_s + \alpha_{s-1}}\Big(1 - \sum_{i=k}^{s} \alpha_i\Big)\Big]$$

$$Q^L_{k+\frac{1}{2}} = \sum_{i=l+1}^{k} \alpha_i Q_i + \Big(1 - \sum_{i=l+1}^{k} \alpha_i\Big) \cdot \Big[Q_l + \frac{Q_{l+1} - Q_l}{\alpha_l + \alpha_{l+1}}\Big(\sum_{i=l}^{k} \alpha_i - 1\Big)\Big]$$

$$Q^R_{k+\frac{1}{2}} = \sum_{i=k+1}^{t-1} \alpha_i Q_i + \Big(1 - \sum_{i=k+1}^{t-1} \alpha_i\Big) \cdot \Big[Q_t + \frac{Q_t - Q_{t-1}}{\alpha_t + \alpha_{t-1}}\Big(1 - \sum_{i=k+1}^{t} \alpha_i\Big)\Big]$$

7.1. Approximation of the advection equation on irregular grids. We will show that these h-box values used in an upwind scheme (which is equivalent to the first order wave propagation algorithm) lead to a consistent approximation of the advection equation $q_t + aq_x = 0$ with $a > 0$. The scheme has the form

$$
\begin{aligned}
Q_k^{n+1} &= Q_k^n - a\frac{\triangle t}{\alpha_k h}\left(Q^L_{k+\frac{1}{2}} - Q^L_{k-\frac{1}{2}}\right)\\
&= Q_k^n - a\frac{\triangle t}{\alpha_k h}\Bigg\{\alpha_k Q_k^n - \sum_{i=m+1}^{l}\alpha_i Q_i^n + \Big(1-\sum_{i=l+1}^{k}\alpha_i\Big)\\
&\qquad\qquad\qquad\cdot\Big[Q_l^n + \frac{Q_{l+1}^n - Q_l^n}{\alpha_l+\alpha_{l+1}}\Big(\sum_{i=l}^{k}\alpha_i - 1\Big)\Big]\\
&\qquad -\Big(1-\sum_{i=m+1}^{k-1}\alpha_i\Big)\Big[Q_m^n + \frac{Q_{m+1}^n - Q_m^n}{\alpha_m+\alpha_{m+1}}\Big(\sum_{i=m}^{k-1}\alpha_i - 1\Big)\Big]\Bigg\}
\end{aligned}
\tag{7.3}
$$

Proposition 3. *The scheme (7.3) leads to a first order accurate approximation of the advection equation on an irregular grid.*

Proof: We will consider the local truncation error of this h-box method. Note that for $i < k$ we have $x_i = x_k - h\left(\frac{1}{2}\alpha_k + \sum_{j=i+1}^{k-1}\alpha_j + \frac{1}{2}\alpha_i\right)$. The Taylor series expansion of the exact solution $q(x_i, t^n)$ at the point x_k has the form

$$
q_i^n = q_k^n - h\Big(\frac{1}{2}\alpha_k + \sum_{j=i+1}^{k-1}\alpha_j + \frac{1}{2}\alpha_i\Big)q_x(x_k,t^n) + \mathcal{O}(h^2).
$$

We will also use the relation

$$
q_{i+1}^n - q_i^n = \frac{1}{2}h(\alpha_{i+1}+\alpha_i)q_x(x_k,t^n) + \mathcal{O}(h^2), \quad (i<k).
$$

Note that the inequalities $m \le l < k$ hold. One time step of the h-box method (7.3) applied to the exact solution $q(x_k, t^n)$ can then be written in the form:

$$
\begin{aligned}
\tilde{q}_k^{n+1} = q_k^n - a\frac{\triangle t}{\alpha_k h}\Big\{&\alpha_k q_k^n - \sum_{i=m+1}^{l}\alpha_i\Big[q_k^n - h\Big(\frac{1}{2}\alpha_k + \sum_{j=i+1}^{k-1}\alpha_j + \frac{1}{2}\alpha_i\Big)q_x(x_k,t^n)\Big]\\
&+\Big(1-\sum_{i=l+1}^{k}\alpha_i\Big)\cdot\Big[q_k^n - h\Big(\frac{1}{2}\alpha_k + \sum_{j=l+1}^{k-1}\alpha_j + \frac{1}{2}\alpha_l\Big)q_x(x_k,t^n)\\
&\qquad\qquad + \frac{1}{2}hq_x(x_k,t^n)\Big(\sum_{i=l}^{k}\alpha_i - 1\Big)\Big]\\
&+\Big(1-\sum_{i=m+1}^{k-1}\alpha_i\Big)\cdot\Big[q_k^n - h\Big(\frac{1}{2}\alpha_k + \sum_{j=m+1}^{k-1}\alpha_j + \frac{1}{2}\alpha_m\Big)q_x(x_k,t^n)\\
&\qquad\qquad + \frac{1}{2}hq_x(x_k,t^n)\Big(\sum_{i=m}^{k-1}\alpha_i - 1\Big)\Big]\Big\} + \triangle t\mathcal{O}(h)
\end{aligned}
$$

$$
\begin{aligned}
&= q_k^n - a\frac{\triangle t}{\alpha_k h}\Big\{\alpha_k q_k^n + \Big(1-\sum_{i=l+1}^{k}\alpha_i\Big)q_k^n - \Big(1-\sum_{i=m+1}^{k-1}\alpha_i\Big)q_k^n - q_k^n\sum_{i=m+1}^{l}\alpha_i \\
&\qquad\qquad + \sum_{i=m+1}^{l}\Big(\alpha_i h\Big(\frac{1}{2}\alpha_k + \sum_{j=i+1}^{k-1}\alpha_j + \frac{1}{2}\alpha_i\Big)q_x(x_k,t^n)\Big) \\
&\quad + \Big(1-\sum_{i=l+1}^{k}\alpha_i\Big)hq_x(x_k,t^n)\Big[\frac{1}{2}\Big(\sum_{i=l}^{k}\alpha_i - 1\Big) - \Big(\frac{1}{2}\alpha_k + \sum_{j=l+1}^{k-1}\alpha_j + \frac{1}{2}\alpha_l\Big)\Big] \\
&\quad - \Big(1-\sum_{i=m+1}^{k-1}\alpha_i\Big)hq_x(x_k,t^n) \\
&\qquad\qquad \cdot\Big[\frac{1}{2}\Big(\sum_{i=m}^{k-1}\alpha_i - 1\Big) - \Big(\frac{1}{2}\alpha_k + \sum_{j=m+1}^{k-1}\alpha_j + \frac{1}{2}\alpha_m\Big)\Big]\Big\} + \triangle t\mathcal{O}(h)
\end{aligned}
\tag{7.4}
$$

The terms in $\{\dots\}$ braces that involve q_k^n have the form

$$
\begin{aligned}
&q_k\Big[\alpha_k + \Big(1-\sum_{i=l+1}^{k}\alpha_i\Big) - \Big(1-\sum_{i=m+1}^{k-1}\alpha_i\Big) - \sum_{i=m+1}^{l}\alpha_i\Big] \\
&= q_k\Big[\alpha_k - \sum_{i=m+1}^{k}\alpha_i + \sum_{i=m+1}^{k-1}\alpha_i\Big] = 0
\end{aligned}
$$

The terms in braces that contain $q_x(x_k,t^n)$ can be simplified in the following way:

$$
\begin{aligned}
I &= hq_x(x_k,t^n)\Big\{\sum_{i=m+1}^{l}\Big[\alpha_i\Big(\frac{1}{2}\alpha_k + \sum_{j=i+1}^{k-1}\alpha_j + \frac{1}{2}\alpha_i\Big)\Big] \\
&\quad + \frac{1}{2}\Big(1-\sum_{i=l+1}^{k}\alpha_i\Big)\cdot\Big(-1-\sum_{i=l+1}^{k-1}\alpha_i\Big) - \frac{1}{2}\Big(1-\sum_{i=m+1}^{k-1}\alpha_i\Big)\cdot\Big(-1-\sum_{j=m+1}^{k}\alpha_j\Big)\Big\} \\
&= hq_x(x_k,t^n)\Big\{\sum_{i=m+1}^{l}\Big[\alpha_i\Big(\frac{1}{2}\alpha_k + \sum_{j=i+1}^{k-1}\alpha_j + \frac{1}{2}\alpha_i\Big)\Big] \\
&\quad + \alpha_k - \frac{1}{2}\alpha_k\sum_{i=m+1}^{l}\alpha_i - \frac{1}{2}\Big(\sum_{j=l+1}^{k-1}\alpha_j\Big)\cdot\Big(\sum_{i=m+1}^{l}\alpha_i\Big) - \frac{1}{2}\Big(\sum_{j=m+1}^{l}\alpha_j\Big)\cdot\Big(\sum_{i=m+1}^{k-1}\alpha_i\Big)\Big\} \\
&\qquad = hq_x(x_k,t^n)\Big\{\sum_{i=m+1}^{l}\Big[\alpha_i\Big(\sum_{j=i+1}^{k-1}\alpha_j + \frac{1}{2}\alpha_i\Big)\Big] \\
&\qquad\quad + \alpha_k - \frac{1}{2}\Big(\sum_{j=l+1}^{k-1}\alpha_j\Big)\cdot\Big(\sum_{i=m+1}^{l}\alpha_i\Big) - \frac{1}{2}\Big(\sum_{j=m+1}^{l}\alpha_j\Big)\cdot\Big(\sum_{i=m+1}^{k-1}\alpha_i\Big)\Big\} \\
&= hq_x(x_k,t^n)\Big\{\sum_{i=m+1}^{l}\Big(\alpha_i\sum_{j=i+1}^{k-1}\alpha_j + \frac{1}{2}\alpha_i\Big) \\
&\qquad \alpha_k - \Big(\sum_{i=m+1}^{l}\alpha_i\Big)\cdot\Big(\sum_{i=l+1}^{k-1}\alpha_i\Big) - \frac{1}{2}\Big(\sum_{i=m+1}^{l}\alpha_i\Big)\cdot\Big(\sum_{i=m+1}^{l}\alpha_i\Big)\Big\}
\end{aligned}
$$

$$= hq_x(x_k,t^n)\Big\{ \sum_{i=m+1}^{l} \Big(\alpha_i \sum_{j=i+1}^{k-1} \alpha_j\Big) + \frac{1}{2}\sum_{i=m+1}^{l} \alpha_i^2$$

$$\alpha_k - \Big(\sum_{i=m+1}^{l}\alpha_i\Big)\cdot\Big(\sum_{i=l+1}^{k-1}\alpha_i\Big) - \frac{1}{2}\sum_{i=m+1}^{l}\alpha_i^2 - \sum_{i=m+1}^{l}\Big(\alpha_i\sum_{j=i+1}^{l}\alpha_j\Big)\Big\}$$

$$= hq_x(x_k,t^n)\Big\{ \sum_{i=m+1}^{l} \Big(\alpha_i \sum_{j=i+1}^{k-1} \alpha_j\Big) + \alpha_k - \Big(\sum_{i=m+1}^{l}\alpha_i\Big)\cdot\Big(\sum_{i=l+1}^{k-1}\alpha_i\Big)\Big\}$$

$$= q_x(x_k,t^n)h\alpha_k$$

Equation (7.4) can therefore be written in the form

$$\tilde{q}_k^{n+1} = q_k^n - a\triangle t q_x(x_k,t^n) + \mathcal{O}(h\triangle t) = q_k^{n+1} + \mathcal{O}(h\triangle t),$$

i.e. the h-box method based on the first order wave propagation algorithm on an arbitrary irregular grid leads to a first order approximation for the advection equation if the h-box values are calculated by averaging over the piecewise linear functions described above. ∎

Using the results of Stern [34], TVD stability of the scheme (7.3) can be shown under some restrictions on the slopes used for the piecewise linear reconstruction. This stability result requires that for the piecewise linear reconstructed values (7.1), (7.2) the inequality $TV(\overline{Q}^n) \leq TV(Q^n)$ holds. Under appropriate smoothness assumptions this TVD property can be obtained without limiting the slopes. Together with the consistency result shown above we obtain first order convergence of the h-box method (7.3).

Once the h-box values are defined we can apply the same second order correction terms (3.9) at the cell interfaces of a completely irregular grid. With such an approach we can expect second order convergence. Figure 7.2 shows numerical results for the approximation of the advection equation on a sequence of irregular grids. The initial

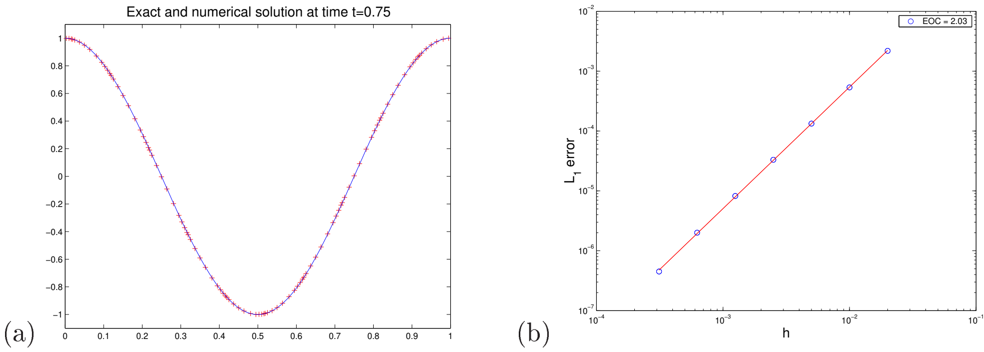

FIG. 7.2. *Approximation of the advection equation on an irregular grid. (a) numerical results on an irregular grid with $h = 0.02$, (b) log-log-plot of h versus L_1-error (EOC = 2.03)*

values are set to $q(x, 0) = \sin(2\pi x)$ on the interval $[0, 1]$. Periodic boundary conditions are imposed. This same example was also considered in Section 2. A convergence study shows that our method converges with second order accuracy. The accuracy of this calculation compares well with the accuracy of the standard wave propagation algorithm considered in Section 2. However, here we could use much larger time steps.

7.2. Approximation of the Euler equations on irregular grids. Now we show the performance of such a high-resolution scheme for some test cases that are modeled by the Euler equations. First we consider the approximation of the smooth test problem defined in Example 6.1 on a completely irregular grid. In Figure 7.3 (a) we show results of the high-resolution h-box method where the h-box values are calculated by averaging over piecewise linear values. Figure 7.3 (b) shows results for the same test calculation, but using cell averaging over piecewise constant cell average values of the conserved quantities in order to calculate the h-box values.

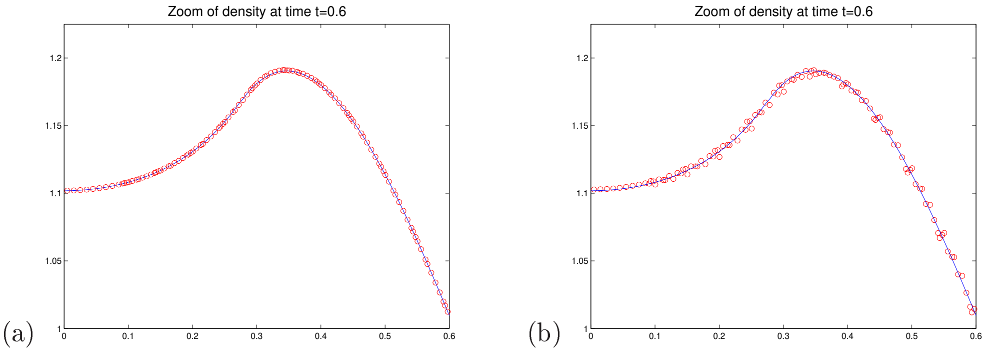

FIG. 7.3. *Numerical results for accuracy test problem approximating Euler equations on a completely irregular grid using the second order accurate method. (a) The h-box values are defined using the interpolation formula (3.3). (b) The h-box values are defined using cell averaging. The solid line is a highly resolved reference solution calculated on an equidistant grid.*

In our next example we consider the approximation of a shock wave solution of the Euler equations.

EXAMPLE 7.1. *We consider the 1D Euler equations with initial values on the interval* $[0, 1]$ *that have constant density* $\rho = 1$ *and constant pressure* $p = 1$. *The velocity is set to* $u = 1$ *for* $x < 0.5$ *and* $u = -1$ *for* $x > 0.5$. *The ratio of specific heats is* $\gamma = 1.05$. *The exact solution of this problem consists of two symmetric shock waves that are propagating outwards. We use an irregular grid with grid cells that may be smaller than* $h = 0.01$ *on the left half of the interval. For* $x > 0.5$ *the grid is regular with mesh length* $\triangle x = 0.01$. *We use time steps that correspond to* $CFL_h \approx 0.9$.

Figure 7.4 shows numerical results of Example 7.1 for the high-resolution h-box method based on the linear interpolation formula. Our numerical results in (a) show that the limiters described in Section 3.3 can suppress spurious oscillations near the discontinuity. The approximation of the shock wave that is moving into the region of the irregular grid is in good agreement with the symmetric shock wave that is moving into the regular part of the grid. On the irregular grid the shock is smeared out over more grid cells than on the regular grid. The reason for this more smeared out shock profile is that a jump in the conserved quantities can have an influence to several h-box values. In Figure 7.4 (b) we show the results obtained by the second order method without limiters.

In Section 5 we pointed out that the h-box method can cause spurious oscillations in the approximation of transonic rarefaction waves for Burgers' equation. This same effect can also be observed in the approximation of a transonic rarefaction wave for the Euler equations. To see this we consider the following example.

EXAMPLE 7.2. *We consider the 1D Euler equations with Riemann initial values of the form* $\rho = 1$, $u = 0.75$, $p = 1$ *for* $x \leq 0.3$ *and* $\rho = 0.125$, $u = 0$, $p = 0.1$ *for*

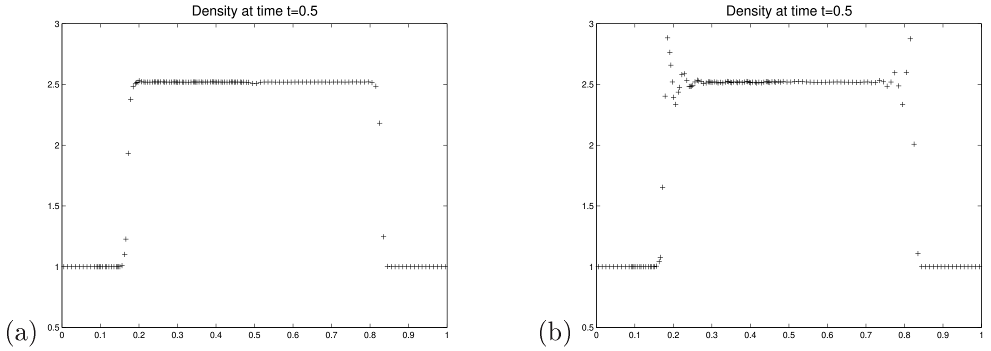

FIG. 7.4. *Approximation of Example 7.1 on a grid that is irregular for $x < 0.5$ and regular for $x > 0.5$. (a) plot of density with limiters, (b) plot of density without limiters.*

$x > 0.3$. The ratio of specific heats is $\gamma = 1.4$. The solution of this Riemann problem consists of a right-moving shock followed by a contact discontinuity and a transonic rarefaction wave. We consider the approximation of this Riemann problem on an irregular grid.

In Figure 7.5 we show the approximation of Example 7.2, where the Roe Riemann solver with entropy fix is used in order to calculate the flux at the cell interfaces. The numerical solution shows some oscillations around the sonic point, see Figure 7.5 (b) which shows a closer view of the region around the sonic point. If the fluxes at the cell interfaces are calculated by the Lax-Friedrichs method this numerical problem does not arise, see Figure 7.6.

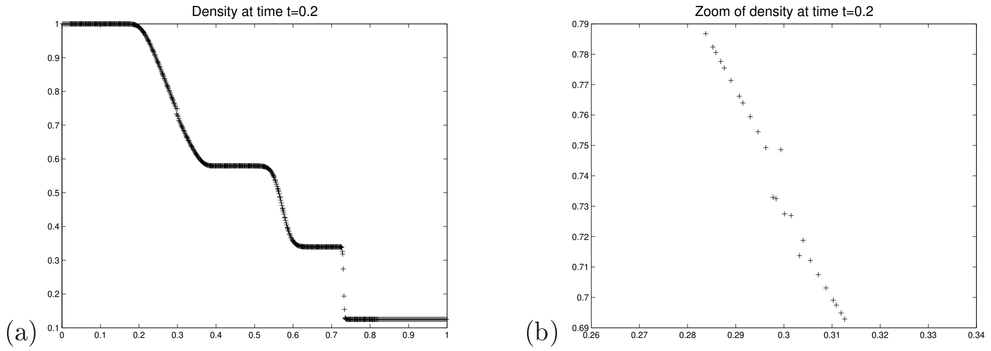

FIG. 7.5. *Approximation of Example 7.2. (a) plot of density obtained by Roe solver with entropy fix, (b) zoom of density around sonic point.*

8. Higher-dimensional irregular grid calculations. Here we will consider two dimensional system of conservation laws in the form

$$\frac{\partial}{\partial t}q(x,y,t) + \frac{\partial}{\partial x}f(q(x,y,t)) + \frac{\partial}{\partial y}g(q(x,y,t)) = 0. \tag{8.1}$$

The simplest way to extend a one dimensional method for conservation laws to multidimensional problems is to use a dimension splitting approach. Then the equation (8.1) would be approximated by solving one dimensional subproblems in an alternating way. In order to obtain multidimensional approximations on an irregular

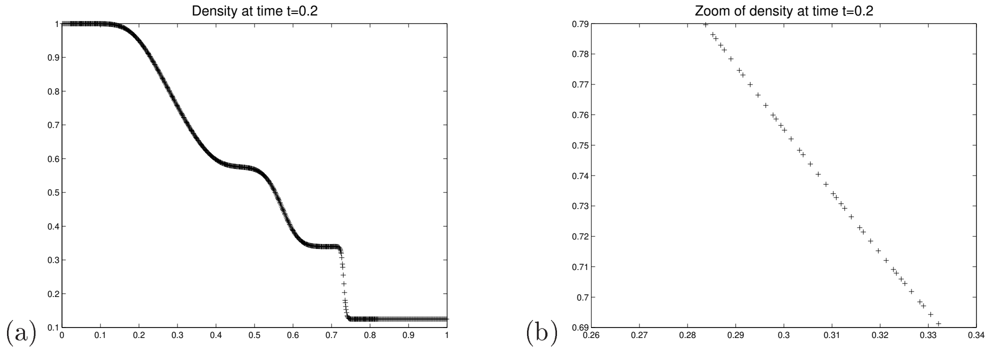

FIG. 7.6. *Approximation of Example 7.2. (a) plot of density obtained by Lax-Friedrichs method, (b) zoom of density around sonic point.*

grid, we can use the high-resolution one-dimensional h-box method, with h-box values defined via the interpolation formula (3.3) and second order correction fluxes of the form (3.9) in each substep.

Instead of using a dimensional splitting approach, we will here develop a two-dimensional h-box method that is based on the multidimensional wave propagation algorithm [22]. We assume that the reader is familiar with the two dimensional wave propagation algorithm described in [22] and outlined briefly in Section 2. See also [21] for a description of the wave propagation algorithm for the advection equation.

As a first step in this approach we solve one-dimensional Riemann problems normal to each cell interface. Based on formula (3.7), which describes the one-dimensional h-box method, we obtain

$$\begin{aligned} Q_{ij}^{n+1} &= Q_{ij}^n + \triangle_{ij}^{up} \\ &= Q_{ij}^n - \frac{\triangle t}{\triangle x_{ij}} \left(\mathcal{A}^+ \triangle \hat{Q}_{i-\frac{1}{2},j} + \mathcal{A}^- \triangle \hat{Q}_{i+\frac{1}{2},j} + f(Q^L_{i+\frac{1}{2},j}) - f(Q^R_{i-\frac{1}{2},j}) \right) \\ &\quad - \frac{\triangle t}{\triangle y_{ij}} \left(\mathcal{B}^+ \triangle \hat{Q}_{i,j-\frac{1}{2}} + \mathcal{B}^- \triangle \hat{Q}_{i,j+\frac{1}{2}} + g(Q^L_{i,j+\frac{1}{2}}) - g(Q^R_{i,j-\frac{1}{2}}) \right) \end{aligned} \tag{8.2}$$

The method (8.2) is stable for time steps that satisfy $\mathrm{CFL_h} \leq \frac{1}{2}$. Second order correction terms of the form (3.9) can be included in x as well as in y direction, which leads to a method of the form

$$Q_{ij}^{n+1} = Q_{ij}^n + \triangle_{ij}^{up} - \frac{\triangle t}{\triangle x_{ij}} \left(\hat{F}^2_{i+\frac{1}{2},j} - \hat{F}^2_{i-\frac{1}{2},j} \right) + \frac{\triangle t}{\triangle y_{ij}} \left(\hat{G}^2_{i,j+\frac{1}{2}} - \hat{G}^2_{i,j-\frac{1}{2}} \right). \tag{8.3}$$

The second order correction terms are again obtained by using the waves and speeds calculated from solving Riemann problems defined by h-box values. Limiters are used in exactly the same form as described earlier for the 1D case.

In addition to fluxes in the normal direction, the multidimensional wave propagation algorithm also calculates waves that are moving in a transverse direction. For the usual wave propagation scheme one has $Q^L_{i+\frac{1}{2},j} = Q^R_{i-\frac{1}{2},j}$ and $Q^L_{i,j+\frac{1}{2}} = Q^R_{i,j-\frac{1}{2}}$. In this case the transverse propagation of waves can be obtained by a decomposition of the flux differences $\mathcal{A}^\pm \triangle Q$, $\mathcal{B}^\pm \triangle Q$ into transverse fluctuations. For the h-box method this transverse propagation has to be modified.

In order to explain the transverse propagation we consider the 2D advection equation

$$\frac{\partial}{\partial t}q(x,y,t) + a\frac{\partial}{\partial x}q(x,y,t) + b\frac{\partial}{\partial y}q(x,y,t) = 0, \qquad a,b > 0.$$

Under the assumption that $\triangle x_{ij} = h$ and $\triangle y_{ij} \le h$, the change of the cell average of the conserved quantity q in grid cell (i,j) due to the first order update in the x direction has the form

$$-\frac{\triangle t}{\triangle h}\mathcal{A}^+\triangle Q_{i-\frac{1}{2},j} = -\frac{\triangle t}{h}a(Q^n_{i,j} - Q^n_{i-1,j}). \tag{8.4}$$

Since we assume that the advection speed a in the x-direction is positive, there is no wave that moves into this cell from the right cell interface. Furthermore, the difference $f(Q^L_{i+\frac{1}{2},j}) - f(Q^R_{i-\frac{1}{2},j})$ vanishes in the case $\triangle x_{ij} = h$. In the 2D case a part of the right-moving flux difference $\mathcal{A}^+\triangle Q$ should affect other grid cells. This is indicated in Figure 8.1. The shaded regions indicate the influence of the jump $Q_{ij} - Q_{i-1,j}$ (initially located at the left cell interface) due to the solution of the Riemann problem in the normal direction. In a multidimensional method the solution of the Riemann problem at the interface $x_{i-\frac{1}{2}}$ should not only affect the cell average of the conserved quantities in the grid cell $(i-1,j)$ and (i,j). It should also have an effect on grid cells in the tangential direction. In the situation shown in (a), the triangular portion of the

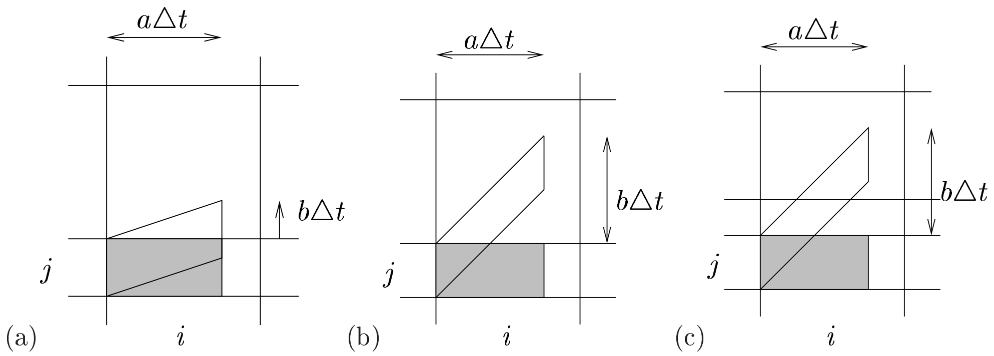

FIG. 8.1. *Different possibilities for transverse propagation of a right-moving wave for the advection equation on a non-uniform Cartesian grid.*

wave describes the fraction that should affect the grid cell $(i, j+1)$. The transverse propagation of the wave considered in Figure 8.1 (a) should change the cell average of the conserved quantity in grid cell (i,j) by the amount

$$\frac{(\triangle t)^2}{\triangle x_{ij}\triangle y_{ij}}\frac{1}{2}b\mathcal{A}^+\triangle Q_{i-\frac{1}{2},j} = \frac{(\triangle t)^2}{\triangle x_{ij}\triangle y_{ij}}\frac{1}{2}\mathcal{B}^+\mathcal{A}^+\triangle Q_{i-\frac{1}{2},j}.$$

The change of the cell average of the conserved quantity in cell $(i, j+1)$ due to the transverse propagation of this wave has the form

$$-\frac{(\triangle t)^2}{\triangle x_{i,j+1}\triangle y_{i,j+1}}\frac{1}{2}\mathcal{B}^+\mathcal{A}^+\triangle Q_{i-\frac{1}{2},j}.$$

The notation $\mathcal{B}^\pm\mathcal{A}^\pm\triangle Q$ was introduced in [22] to describe transverse propagations of left and right moving flux differences. For the wave propagation algorithm with time step restriction CFL ≤ 1 the transverse propagation has always the triangular form depicted in Figure 8.1 (a), even if the grid is irregular. Since the transverse propagation approximates terms that are needed in order to obtain second order accuracy, we include those terms into the second order correction terms used in Equation (8.3). The up-going flux difference $\mathcal{B}^+\mathcal{A}^+\triangle Q_{i-\frac{1}{2}}$ contributes to the $\tilde{G}$ term in the form of an update

$$\hat{G}^2_{i,j+\frac{1}{2}} := \hat{G}^2_{i,j+\frac{1}{2}} - \frac{1}{2}\frac{\triangle t}{\triangle x_{ij}}\mathcal{B}^+\mathcal{A}^+\triangle Q_{i-\frac{1}{2},j}$$

For our h-box method we have to extend the transverse propagation to allow also wave propagation of other forms, for instance those shown in (b) or (c). For the situation shown in Figure 8.1 (b) the update of the flux $\tilde{G}$ due to the transverse propagation has the form

$$\hat{G}^2_{i,j+\frac{1}{2}} := \hat{G}^2_{i,j+\frac{1}{2}} - \frac{\triangle t - \frac{1}{2}\triangle y_{ij}/b}{b}\triangle y_{ij}\mathcal{B}^+\mathcal{A}^+\triangle Q_{i-\frac{1}{2},j}.$$

In the situation shown in (c), the transverse propagation of $\mathcal{A}^+\triangle Q_{i-\frac{1}{2},j}$ leads to an update of $\hat{G}^2_{i,j+\frac{1}{2}}$ as well as $\hat{G}^2_{i,j+\frac{3}{2}}$, depending on the fraction of the wave considered. As demonstrated in these examples, simple geometric routines can be used to calculate the fraction of the waves that determine the change of the cell average of the conserved quantity due to the transverse propagation. Note that the wave speed in the normal direction (i.e. a in our example) is present in the fluctuations $\mathcal{A}^\pm\triangle Q$. In order to calculate the transverse propagations no other information from the structure of the Riemann problem in normal direction is needed. Therefore, even for a system of conservation laws, we only have to decompose the left and right-moving flux differences, instead of decomposing each wave resulting from the Riemann problem in normal direction separately.

So far we have assumed that $\triangle x_{ij} = h$. If $\triangle x_{ij} < h$, we want to use the one-dimensional h-box method in order to calculate the fluxes in the normal direction. The transverse propagation will take a very similar form as discussed above. Now we could interpret the grid cells (i,j), $(i,j+1)$ shown in Figure 8.1 as h-boxes constructed at the interface $x_{i-\frac{1}{2}}$. The transverse propagation of waves should again depend on the fraction of the wave that moves through the h-box considered. This can be calculated in exactly the same way as described above for the case $\triangle x_{ij} = h$. In order to obtain the correct cancellation property needed for a stable update, we have to include the terms $f(Q^L_{i+\frac{1}{2},j})$ and $f(Q^R_{i-\frac{1}{2},j})$ that arise in Equation (8.2) into our transverse propagation. Motivated by equations (2.1), (2.2) we do this by applying an update of the form

$$\begin{aligned}
\mathcal{A}^+\triangle Q_{i-\frac{1}{2},j} &:= \mathcal{A}^+\triangle Q_{i-\frac{1}{2},j} - f(Q^R_{i-\frac{1}{2}})\\
\mathcal{A}^-\triangle Q_{i-\frac{1}{2},j} &:= \mathcal{A}^-\triangle Q_{i-\frac{1}{2},j} + f(Q^L_{i-\frac{1}{2}})
\end{aligned}$$

before we calculate the change of the fluxes $\hat{G}^2$. For our example of the advection equation with positive advection speeds, this update of $\mathcal{A}^\pm\triangle Q$ has the effect that $\mathcal{A}^-\triangle Q$ is no longer equal to zero. Moreover, the fraction of the wave that is propagated in the transverse direction only depends on the size of the grid cells and the speed b. Therefore, our transverse propagation has the effect that a fraction of the update used in Equation (8.3) is propagated in the transverse direction. The update, which describes the wave propagation in the x direction was already constructed to be of the order $\mathcal{O}(\triangle x)$ with $\triangle x \le h$. Our transverse propagation allows that at most a fraction of magnitude $\mathcal{O}(\triangle y)$ $(\triangle y \le h)$ is propagated in transverse direction. (See for instance Figure 8.1 (c).) Therefore, our transverse propagation satisfies the cancellation property. The transverse propagation of $\mathcal{B}^+\triangle Q$ also has to be included in an analogous way. By including the transverse propagation into our 2D h-box method, we obtain stability for time steps that satisfy the condition $\mathrm{CFL_h} \le 1$.

A transverse propagation of the second order correction (3.9) can be included into the transverse propagation in the same form as it was discussed for the wave propagation algorithm in [22]. This further increases the accuracy of the method. It was used in our test calculations below.

We now demonstrate the performance of our 2D high-resolution h-box method for the approximation of the advection equation. We will compare the numerical results obtained for this h-box scheme with results obtained using the standard high-resolution CLAWPACK algorithm for irregular grid calculations. The latter method requires the time step restriction $\mathrm{CFL} \le 1$, while the h-box method is stable for time steps that satisfy $\mathrm{CFL_h} \le 1$. We first study the accuracy for the two dimensional advection equation.

EXAMPLE 8.1. *We consider the approximation of the advection equation* $q_t + q_x + q_y = 0$, *with initial values* $q(x, y, 0) = \sin(2\pi x)\cos(2\pi y)$ *on the domain* $[0, 1] \times [0, 1]$. *We impose periodic boundary conditions. The grid contains two lines as well as two columns of grid cells with height respectively width* $0.1h$ *and* $0.9h$. *All other grid cells have the size* $h \times h$. *See Figure 8.2 (a) for a plot of a fraction of the grid.*

Test calculations for Example 8.1 confirm that the h-box method leads to second order accurate approximations also in this multidimensional application. In Figure 8.2 (d) we document the experimental order of convergence of the h-box method in both the L_1-norm (depicted by o-symbols) as well as in the maximum norm (+-symbols). For this grid, inaccuracies near the small cells would be displayed in the maximum norm rather than the L_1-norm. However, in both norms the experimental order of convergence is about 2. The results for the h-box method compare well with numerical results obtained with the standard wave propagation algorithm with appropriate modifications that allow the approximation on a nonuniform grid. Both schemes converge with second order, but the error is slightly smaller if we use the h-box method. This is due to the numerical viscosity, since the time step restriction $\mathrm{CFL} \approx 0.9$ for the wave propagation algorithm leads away from the small cell to time steps that correspond to $\mathrm{CFL} \le 0.1$.

Our two-dimensional h-box method can be extended to systems of conservation laws in the same way as the standard wave propagation algorithm. The modifications described above now have to be applied to each wave resulting from the decomposition of the left- respectively right-going flux differences into up- and down-going waves.

In our last example we consider the approximation of a two dimensional Riemann problem for the Euler equations, as studied in [33] . This same example was considered in [22], where results of CLAWPACK calculations on a uniform grid are shown. The initial values are piecewise constant in four quadrants and the solution of each single Riemann problem is a shock wave. Due to the interaction a complex solution structure is obtained. For this calculation we have, in addition to the regular grid cells of the size $h \times h$, 10 lines and 10 columns with height respectively width varying between $0.1h$ and $0.9h$. Our solution on a nonuniform grid calculated by the high-resolution h-box method with $h = 0.005$ compares well with those obtained on a regular grid.

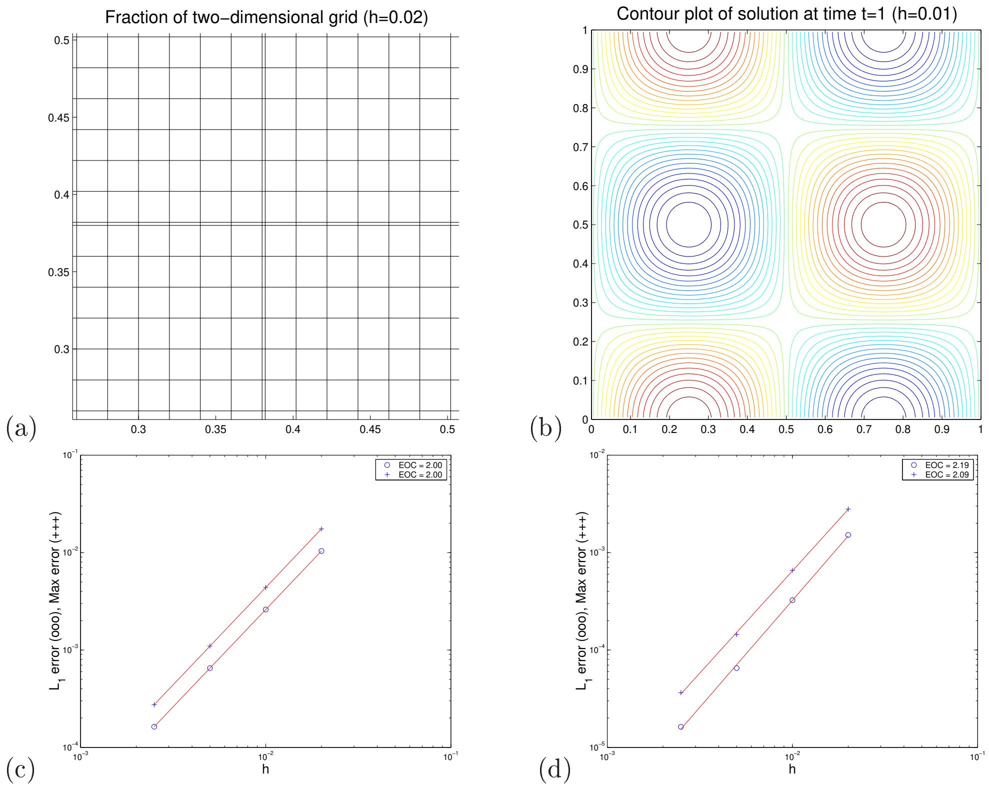

FIG. 8.2. *Approximation of Example 8.1. (a) The grid for a discretization with* $h = 0.02$*, (b) contour plot of the solution using the two-dimensional* h*-box approach with* $h = 0.01$ *and* $CFL_h \approx 0.9$*, (c) convergence study for irregular grid* CLAWPACK *algorithm using* $CFL \approx 0.9$*, (d) convergence study for* h*-box method using* $CFL_h \approx 0.9$*. (o-symbol: error in* L_1*-norm, +-symbol: error in maximum norm)*

See Figure 8.3 for a comparison of both calculations.

Conclusions. We studied high-resolution h-box methods for the approximation of hyperbolic systems of conservation laws on irregular grids. The special construction of these schemes with flux calculations based on Riemann problems defined over boxes of length h allows time steps that are appropriate for regular parts of the grid in situations where some grid cells may be orders of magnitude smaller than those regular or reference grid cells.

The definition of the h-box values is important in order to construct accurate schemes. We describe an h-box method that leads to a second order accurate approximation of the advection equation on irregular grids without any smoothness assumptions on the grid. We show by numerical experiments that this scheme also leads to a high-resolution approximation for the Euler equations.

The entropy-consistency of the scheme was discussed for the approximation of Burgers' equation. In contrast to the classical Godunov scheme, the h-box method can lead to numerical problems for the approximation of transonic rarefaction waves if the fluxes at the interfaces of the irregular grid cells are approximated by using an exact solver. The same difficulty can also be observed in the approximation of transonic rarefaction waves for the Euler equations. This numerical problem in the

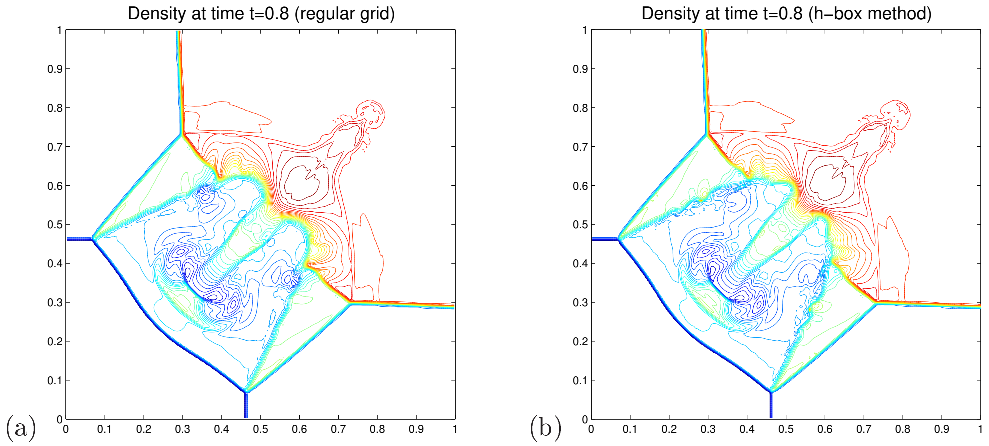

FIG. 8.3. *(a) Contour plot of density obtained by the high-resolution wave propagation algorithm on a uniform grid with* $h = 0.005$*, (b) contour plot of density obtained with high-resolution* h*-box method,* $h = 0.005$*. We used the monotonized centered limiter.*

approximation of transonic rarefaction waves can be avoided by replacing the Godunov flux by the Lax-Friedrichs flux.

In forthcoming work we construct a new two-dimensional h-box scheme for the approximation of conservation laws with embedded irregular boundaries. In [6] and [7], Berger and LeVeque constructed such a scheme based on a rotated grid h-box method. In our new scheme h-boxes at embedded boundaries will be constructed in coordinate directions which allows a more direct use of the high-resolution scheme described here. Some preliminary results are presented in [3].

Appendix A. Stability of the second order h-box method. In this appendix we prove the stability of the second order h-box scheme for $q_t = q_x$ using linear interpolation according to the theory of Gustafsson, Kreiss and Sundstrom [13] (henceforth GKS). We treat the small cell with mesh width αh as a boundary condition for the Lax-Wendroff scheme applied on either side of the small cell, using the notation of Figure A.1. Here the conserved quantity assigned to the right h-box at

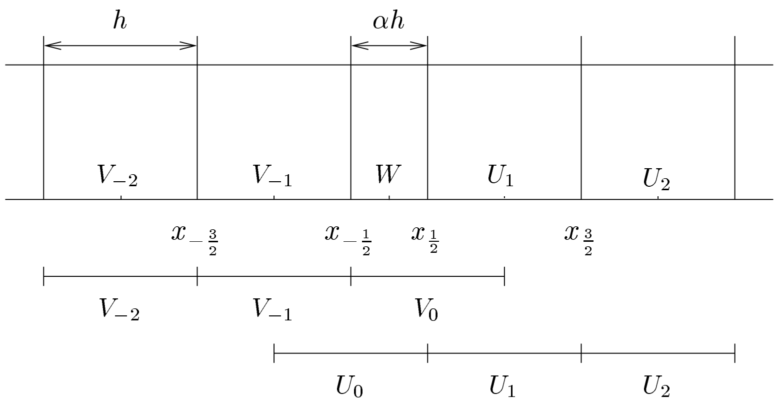

FIG. A.1. *Notation for GKS stability, with one small cell in the middle.*

the interface $x_{-\frac{1}{2}}$ is denoted by V_0. The left h-box value at the interface $x_{\frac{1}{2}}$ is U_0.

The derivation of the stability condition for the update of the small cell is similar to those used in Berger [2], where stability for schemes with local grid refinement was analyzed.

Both U and V are computed using the second order Lax-Wendroff scheme,

$$\begin{aligned} U_j^{n+1} &= U_j^n + \lambda/2(U_{j+1}^n - U_{j-1}^n) + \lambda^2/2(U_{j+1}^n - 2U_j^n + U_{j-1}^n), \qquad j \geq 1, \\ V_j^{n+1} &= V_j^n + \lambda/2(V_{j+1}^n - V_{j-1}^n) + \lambda^2/2(V_{j+1}^n - 2V_j^n + V_{j-1}^n), \qquad j \leq -1, \end{aligned} \tag{A.1}$$

with $\lambda = \frac{\triangle t}{h}$. Using the approach of [2], we look for solutions of the form

$$\begin{aligned} U_j^n &= \rho\kappa^j z^n, |\kappa| \leq 1 \qquad j = 1, 2, \ldots \\ V_j^n &= \sigma\tau^j z^n, |\tau| \geq 1 \qquad j = -1, -2, \ldots. \end{aligned} \tag{A.2}$$

With this numbering, for l_2 solutions the root κ of the characteristic equation for U on the right side has magnitude less than 1, and τ has magnitude greater than 1. Roughly speaking, the scheme is unstable if and only if there are l_2 solutions satisfying the interpolation conditions with growth in time $|z| > 1$.

The linear interpolation conditions (3.3) give us

$$\begin{aligned} U_0 &= \frac{1-\alpha}{1+\alpha} V_{-1} + \frac{2\alpha}{1+\alpha} W \\ V_0 &= \frac{1-\alpha}{1+\alpha} U_1 + \frac{2\alpha}{1+\alpha} W \end{aligned} \tag{A.3}$$

where the small cell, labeled W above, satisfies the "small-cell" version of Lax-Wendroff,

$$W^{n+1} = W^n + \frac{\Delta t}{\alpha h}\left[\frac{U_0+U_1}{2} + \frac{\Delta t}{2h}(U_1 - U_0) - \frac{V_0 + V_{-1}}{2} - \frac{\Delta t}{2h}(V_0 - V_{-1})\right]. \tag{A.4}$$

The characteristic equation for W is $W^n = \hat{w}z^n$. We normalize the equations and take $\hat{w} = 1$. Substituting the characteristic roots for U, V into the interpolation conditions (A.3) gives

$$\begin{aligned} \rho &= \frac{1-\alpha}{1+\alpha}\sigma\tau^{-1} + \frac{2\alpha}{1+\alpha} \\ \sigma &= \frac{1-\alpha}{1+\alpha}\rho\kappa + \frac{2\alpha}{1+\alpha}. \end{aligned} \tag{A.5}$$

Equation (A.5) is easily solved for ρ and σ, giving

$$\begin{aligned} \rho &= \frac{2\alpha\left(1+\alpha+(1-\alpha)\tau^{-1}\right)}{(1+\alpha)^2 - (1-\alpha)^2\kappa\tau^{-1}} \\ \sigma &= \frac{2\alpha\left(1+\alpha+(1-\alpha)\kappa\right)}{(1+\alpha)^2 - (1-\alpha)^2\kappa\tau^{-1}} \end{aligned} \tag{A.6}$$

which we will use later.

Substitution of the resolvent equations for U and V into (A.4) gives

$$z = 1 + \frac{\lambda}{2\alpha}\left[\rho(1+\kappa) + \lambda\rho(\kappa - 1) - \sigma(1+\tau^{-1}) - \lambda\sigma(1-\tau^{-1})\right]. \tag{A.7}$$

We use (A.5) to replace ρ and σ in terms of $\sigma\tau^{-1}$ and $\rho\kappa$. Also, for a given mesh width h on both the left and right, it is easily seen that the product of the roots κ and τ are $\kappa\tau = \frac{\lambda-1}{\lambda+1}$, so τ^{-1} can be replaced using κ in (A.7). Thus, (A.7) simplifies to

$$z = 1 - \frac{2\lambda^2}{1+\alpha} + \frac{\lambda(1+\lambda)}{1+\alpha}\kappa(\rho+\sigma) \tag{A.8}$$

We call this *root condition* for the stability of the small cell scheme with Lax-Wendroff. If there are roots z with $|z| > 1$ and κ, τ^{-1} with magnitude less than or equal to 1, satisfying (A.8) then by the GKS theory, the scheme is unstable. Conversely, if there are no such roots, the scheme is stable. As in [2], we will use the maximum principle to reduce the range of values we need to check for stability.

To see that the maximum principle applies, we will show that the right hand side of (A.8), call it $f(z)$, has no singularities for $|z| \geq 1$ and is bounded as $z \to \infty$. First note that $f(z) = (1 - \frac{2\lambda^2}{1+\alpha}) + \frac{\lambda(1+\lambda)}{1+\alpha}\kappa(\rho+\sigma)$ has no branch points for $|z| \geq 1$. This is because the roots κ, τ satisfy the Lax Wendroff characteristic equation for (A.1),

$$z = 1 + \frac{\lambda}{2}(\eta - \eta^{-1}) + \frac{\lambda^2}{2}(\eta - 2 + \eta^{-1}) \tag{A.9}$$

which lead to a quadratic equation for η with roots

$$\eta_{1,2} = \frac{z - 1 + \lambda^2 \pm \sqrt{(z-1)^2 + \lambda^2(2z-1)}}{\lambda(\lambda+1)} \tag{A.10}$$

One of the roots is always inside the unit circle, the other one is outside the unit circle, see [13], Lemma 6.1. The root inside the unit circle is the root we call κ above, τ is the root that is outside the unit circle.

The square root term of (A.10) is zero only for $z = 1 - \lambda$, which being inside the unit circle is outside the region of interest, so there are no branch points for $|z| > 1$. Also, note from (A.10) that as $z \to \infty$, the root τ grows like $\frac{2z}{\lambda^2+\lambda}$, so the root κ grows like $\frac{\lambda(\lambda-1)}{2z}$, which is clearly bounded for large z. So the maximum principle applies.

Thus $f(z)$ attains its maximum value on the circle $|z| = 1$. The next step then is to examine the magnitude of $f(z)$ for values of z on the unit circle. Since we can only show analytically that $f(z) \leq 1$ for $\lambda > .5$, we instead evaluate $f(z)$ numerically, for $0 \leq \alpha \leq 1$, and $0 < \lambda \leq 1$, on the unit circle for $z = e^{i\theta}, 0 \leq \theta \leq 2\pi$. Figure A.2 shows the locus of values of $f(z)$, where the unit circle is also drawn. As the figure and some algebra shows, only for $z = 1, \lambda = 0$, and $z = -1, \lambda = 1$, does $z = f(z)$.

Examining the first value $z = 1 = f(z)$, we have $\lambda = 0$, or equivalently $\Delta t = 0$, so $Q^{n+1} = Q^n$ (with $Q \in \{U, V, W\}$), clearly a stable solution. For the other case, we have $z = -1 = f(z)$, whose only solution (again using some numerical evaluation and some algebra) is $\lambda = 1, \alpha = 0$. But $\alpha = 0$ corresponds to the usual Lax-Wendroff scheme without the small cell, and $\lambda = 1$ for this case is straight copying of the solution ($\kappa = 0, \tau = -1$). Again this is stable.

REFERENCES

[1] B. Alpert, L. Greengard, and T. Hagstrom. An integral evolution formula for the wave equation. *J. Comput. Phys.*, 162:536–543, 2000.

[2] M.J. Berger. Stability of interfaces with mesh refinement. *Math. Comp.*, 45:301–318, 1985.

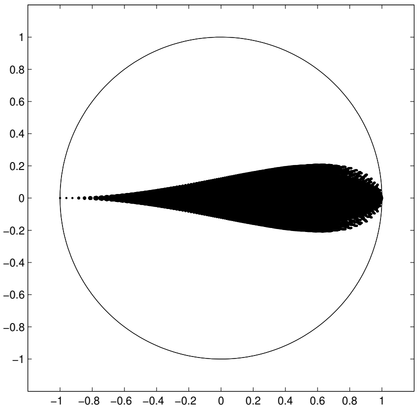

FIG. A.2. *Locus of values of $f(z)$ for $|z| = 1$; all values lie inside or on the unit circle.*

[3] M.J. Berger and C. Helzel. Grid aligned h-box methods for conservation laws in complex geometries. Submitted: Proc. 3rd Intl. Symposium on Finite Volumes for Complex Applications, Porquerolles, France June 2002.

[4] M.J. Berger and R.J. LeVeque. An adaptive Cartesian mesh algorithm for the Euler equations in arbitrary geometries. *AIAA paper AIAA-89-1930*, pages 305–311, 1989.

[5] M.J. Berger and R.J. LeVeque. Cartesian meshes and adaptive mesh refinement for hyperbolic partial differential equations. In *Proc. 3rd Intl. Conf. Hyperbolic Problems, Uppsala, Schweden*, 1990.

[6] M.J. Berger and R.J. LeVeque. Stable boundary conditions for Cartesian grid calculations. *Computing Systems in Engineering*, 1:305–311, 1990.

[7] M.J. Berger and R.J. LeVeque. A rotated difference scheme for Cartesian grids in complex geometries. *AIAA Paper CP-91-1602*, 1991.

[8] M.J. Berger, R.J. LeVeque, and L.G. Stern. Finite volume methods for irregular one-dimensional grids. In *Mathematics of Computation 1943-1993: a half century of computational mathematics, Proc. of Symposia in Applied Mathematics*, volume 48, pages 255–259, 1994.

[9] D. Calhoun and R.J. LeVeque. A Cartesian grid finite-volume method for the advection diffusion equation in irregular geometries. *J. Comput. Phys.*, 157:143–180, 2000.

[10] C.M. Dafermos. *Hyperbolic conservation laws in continuum physics.* Springer, 2000.

[11] J. Falcovitz, G. Alfandary, and G. Hanoch. A two-dimensional conservation laws scheme for compressible flows with moving boundaries. *J. Comput. Phys.*, 138:83–102, 1997.

[12] H. Forrer and R. Jeltsch. A high-order boundary treatment for Cartesian-grid methods. *J. Comput. Phys.*, 140:259–277, 1998.

[13] B. Gustafsson, H.-O. Kreiss, and A. Sundström. Stability theory of difference approximations for mixed initial boundary value problems. II. *Math. Comp.*, 26:649–686, 1972.

[14] A. Harten, P.D. Lax, and B. van Leer. On upstreem differencing and Godunov-type schemes for hyperbolic conservation laws. *SIAM Review*, 25:35–61, 1983.

[15] H. O. Kreiss, T. A. Manteuffel, B. Swartz, B. Wendroff, and A. B. White. Supra-convergent schemes on irregular grids. *Math. Comp.*, 47:537–554, 1986.

[16] R.J. LeVeque. CLAWPACK software. available from `http://www.amath.washington.edu/~ claw/`.

[17] R.J. LeVeque. Large time step shock-capturing techniques for scalar conservation laws. *SIAM J. Numer. Anal.*, 19:1091–1109, 1982.

[18] R.J. LeVeque. Convergence of a large time step generalization of godunov's method for conservation laws. *Comm. Pure Appl. Math.*, 37:463–477, 1984.

[19] R.J. LeVeque. A large time step generalization of Godunov's method for systems of conservation laws. *SIAM J. Num. Anal.*, 22:1051–1073, 1985.

[20] R.J. LeVeque. *Numerical Methods for Conservation Laws.* Birkhäuser Verlag, 1990.

[21] R.J. LeVeque. High-resolution conservative algorithms for advection in incompressible flow. *SIAM J. Numer. Anal.*, 33:627–665, 1996.

[22] R.J. LeVeque. Wave propagation algorithms for multidimensional hyperbolic systems. *J. Comput. Phys.*, 131:327–353, 1997.

[23] R.J. LeVeque. *Finite Volume Methods for Hyperbolic Problems.* Cambridge University Press, 2002.

[24] J.R. Li and L. Greengard. Strongly consistent marching schemes for the wave equation. submitted 2002.

[25] T. A. Manteuffel and A. B. White, Jr. The numerical solution of second-order boundary value problems on nonuniform meshes. *Math. Comp.*, 47:511–535, 1986.

[26] D. Modiano and P. Colella. A higher-order embedded boundary method for time dependent simulation of hyperbolic conservation laws. In *Proceedings of the FEDSM 00 - ASME Fluids Engineering Simulation Meeting*, 2000.

[27] K.W. Morton. On the analysis of finite volume methods for evolutionary problems. *SIAM J. Numer. Anal.*, 35:2195–2222, 1998.

[28] R.B. Pember, J.B. Bell, P. Colella, and W.Y. Crutchfield amd M.L.Welcome. An adaptive Cartesian grid method for unsteady compressible flow in irregular regions. *J. Comput. Phys.*, 120:278–304, 1995.

[29] J. Pike. Grid adaptive algorithms for the solution of the Euler equations on irregular grids. *J. Comput. Phys.*, 71:194–223, 1987.

[30] J.J. Quirk. An alternative to unstructured grids for computing gas dynamic flows around arbitrarily complex two-dimensional bodies. *Computers Fluids*, 23:125–142, 1994.

[31] P.L. Roe. Approximate Riemann solver, parameter vectors, and difference schemes. *J. Comput. Phys.*, 43:357–372, 1981.

[32] M.E. Schonbek. Second order conservative schemes and the entropy condition. *Math. Comp.*, 44:31–38, 1985.

[33] C.W. Schultz-Rinne, J.P. Collins, and H.M. Glaz. Numerical solution of the Riemann-problem for two-dimensional gas dynamics. *SIAM J. Sci. Comput.*, 14:1394–1414, 1993.

[34] L.G. Stern. *An explicit conservative method for time accurate solution of hyperbolic partial differential equations on embedded Chimera grids.* PhD thesis, University of Washington, 1996. `ftp://www.amath.washington.edu/pub/rjl/students/stern:thesis.ps.gz`.

[35] B. van Leer. Towards the ultimate conservative difference scheme II. Monotonicity and conservation combined in a second order scheme. *J. Comput. Phys.*, 14:361–370, 1974.

[36] B. Wendroff and A.B. White. Some supraconvergent schemes for hyperbolic equations on nonuniform grids. In *Proc. Second International Conference on Hyperbolic Problems, Aachen*, pages 671–677, 1988.

[37] B. Wendroff and A.B. White. A supraconvergent scheme for nonlinear hyperbolic systems. *Comput. Math. Appl.*, 18:761–767, 1989.